MAX-PLANCK-INSTITUT FÜR PLASMAPHYSIK

GARCHING BEI MÜNCHEN

Graphs of Anomalous Energy Confinement Times for ASDEX, INTOR, JET, PLT, TFTR and ZEPHYR

H.K. Wimmel

IPP 6/200 July 1980

Die nachstehende Arbeit wurde im Rahmen des Vertrages zwischen dem Max-Planck-Institut für Plasmaphysik und der Europäischen Atomgemeinschaft über die Zusammenarbeit auf dem Gebiete der Plasmaphysik durchgeführt.

IPP 6/200

Graphs of Anomalous Energy Confinement Times for ASDEX, INTOR, JET, PLT, TFTR, and ZEPHYR

H.K. Wimmel

July 1980 (in English)

Abstract

Anomalous transport due to the dissipative trapped-ion instability, anomalous heat conductivity of electrons, and neoclassical heat conductivity of ions are considered. The energy confinement time resulting from the combined effects is represented graphically as a function of the mean temperature and for several values of the mean density for the following tokamaks: ASDEX, INTOR, JET, PLT, TFTR, and ZEPHYR.

1. Introduction

Anomalous transport due to the dissipative trapped-ion instability has not been detected so far in tokamak experiments. On the other hand, one is interested in forecasting energy confinement times τ_E for existing devices at higher temperatures, not yet reached, and for tokamaks not yet in existence, but being planned, designed or built. For this purpose, anomalous trapped-particle transport should also be taken into account.

This report presents τ_E (T) plots for the tokamaks ASDEX, INTOR, JET, PLT, TFTR and ZEPHYR for several mean densities and for r_n/a = 0.5 and 1.0. The confinement times are calculated from a zero-dimensional model. The transport processes considered are:

a) trapped-particle anomalous energy transport due to the dissipative trapped-ion instability [1,2],

b) anomalous heat conductivity of electrons [3,4,5],

c) neoclassical ion heat conductivity [6].

It should be obvious that a zero-dimensional calculation can only give a rough estimate. For more accurate information one has to invoke a self-consistent numerical transport code in at least one spatial dimension.

In Sec. 2 the transport formulas used in evaluating τ_E are listed. The τ_E (T) plots for the six tokamaks considered are discussed in Sec. 3. Tables I to VI list the machine parameters of the six tokamaks. Figures 1 to 36 present the τ_E (T) plots, there being six plots for each of the six tokamaks.

2. Formulas for the Energy Confinement Time

Under the assumptions mentioned in the Introduction the combined energy confinement time τ_E^{TOT} of the plasma is given by

$$\frac{1}{\tau_E^{TOT}} = \frac{1}{\tau_E^{SW}} + \frac{1}{\tau_E^{DP}} + \frac{1}{\tau_E^{NC}} \quad , \tag{2.1}$$

where τ_E^{SW} is the trapped-particle τ_E as given by Sardei and Wimmel [1,2], τ_E^{DP} is the anomalous electron τ_E as given by Düchs, Pfirsch et al. [3,4,5], and τ_E^{NC} is the neoclassical τ_E [6].

The trapped-particle energy confinement time is defined relative to the total energy content of the plasma by the formula [1,2]

$$\tau_E^{SW} = \frac{r_n\, a}{2\, D_s} \quad . \tag{2.2}$$

Here $r_n = |N/N'|$ is the scale length of the radial density variation, a is the minor plasma radius, and D_s is the average anomalous diffusion coefficient due to the dissipative trapped-ion instability, the effect of shear being taken into account. The quantity D_s is given by [1,2]

$$D_s \approx 3.5 \times 10^{-2}\, \delta_o\, \nu_i\, (\Delta a)^2 \tag{2.3}$$

within the existence range of the instability (see below), where $\delta_o = n^o/N$ is the relative number of trapped particles, $\nu_i = \nu_i^{90°}/\delta_o^{\,2}$ is the effective collision frequency of the trapped ions, and Δa is the distance between properly chosen mode-rational surfaces (with $K_\parallel = 0$), viz.

$$\Delta a = \min\left\{ a,\ r_q,\ \frac{r_q}{m_{dom}} \right\} . \tag{2.4}$$

Here $r_q = |q/q'|$ is the radial scale length of the safety factor q,

$m_{dom} \approx 4\, m_{marg}$ is the dominant poloidal mode number, with m_{marg} given by

$$m_{marg} = \frac{a}{2\vartheta_0}\sqrt{\nu_e \nu_i} \quad , \tag{2.5}$$

ν_e is the effective collision frequency of the trapped electrons, and

$$\vartheta_0 = \frac{\delta_0\, c\, T}{2 e B (1-\delta_0)} \quad , \quad T = \frac{2 T_i T_e}{T_i + T_e} \quad , \tag{2.6}$$

with T_j = average temperatures in erg, B = magnetic field in gauss, e = proton charge in esu and c = 3.10^{10} cm/s. The above formulas otherwise all use cgs units. The numerical evaluation of τ_E^{SW} uses an average density N and assumes $T_i = T_e = T$, $\eta \equiv d \ln T / d \ln N = 1$, and $Z_{eff} = 1$. For tokamaks with noncircular cross-sections the minor radius a is replaced by an average radius $\bar{a}_{sw}$ whose definition is adapted to the above formulas, viz.

$$\bar{a}_{sw} = 2^{1/4}\, a_H a_V \left(a_H^4 + a_V^4\right)^{-1/4} \quad , \tag{2.7}$$

with a_H = horizontal minor radius and a_V = vertical minor radius. The quantity δ_0 is then calculated at $r = a_H/2$, viz.

$$\delta_0 = \sqrt{\frac{a_H}{2R}} \quad . \tag{2.8}$$

The existence range of the dissipative trapped-ion instability is given by the conditions [1,7]: $2\pi \nu_j < \omega_{bj}$ (j = i,e), $\omega_{dom} < \omega_{bj}$, $K_y R_i < \pi$, and $K_x R_{Bi} < \pi$ for the dominant mode. Here ω_{bj} are the bounce frequencies of the trapped particles, R_i is the gyro-radius of the ions, and R_{Bi} is the banana width of the trapped ions. If any of these conditions is violated, then the approximation $D_s = 0$, $\tau_E^{SW} = \infty$ is used instead of eq. (2.3).

The anomalous electron energy confinement time was given by Düchs, Pfirsch et al. [3,4,5]. Relative to the total plasma energy, with $T_i = T_e$ assumed, it is given by

$$\tau_E^{DP} = 39.50\ T_e^{1.000}\ N^{0.835}\ B^{-0.912}\ Z_{eff}^{-0.522}$$

$$\times\ q_a^{1.04}\ A^{1.68}\ a^{2.28}\ . \qquad (2.9)$$

Here τ_E^{DP} is given in ms, T_e is the average electron temperature in keV, N is the average density in units of (10^{13} cm^{-3}), B is the magnetic field in tesla, q_a is the safety factor at r = a, A is the aspect ratio, and a is the minor plasma radius in m. The confinement time $\tau_E^{DP} \approx 2\tau_{Ee}$ relates the energy flux to the total thermal energy of both ions and electrons. Again, $T_i = T_e = T$ and $Z_{eff} = 1$ is assumed in the evaluation. For tokamaks with noncircular cross-sections the minor radius a is here replaced by an average radius $\bar{a}_{DP}$ whose definition is approximately adapted to the scaling of eq.(2.9), viz.

$$\bar{a}_{DP} = \sqrt{2}\ a_H\ a_V \left(a_H^2 + a_V^2\right)^{-1/2}\ , \qquad (2.10)$$

where a_H and a_V have been explained above. In addition, the definition $A = R/a_H$ of the aspect ratio was used in these cases. Equation (2.9) involves a best fit of experimental data of many tokamaks with a statistical error of about 20% [3,4,5]. The T-dependence of τ_E^{DP} was inferred from results obtained with the PLT heating experiment [9].

The neoclassical energy confinement time of the ions, re-normalized to the total plasma energy, with $T_i = T_e$ assumed, can be defined as

$$\tau_E^{NC} = \frac{3 N r_T a}{2 \kappa_i}\ , \qquad (2.11)$$

where $r_T = |T/T'|$ is the scale length of the radial temperature

variation, and the thermal conductivity κ_i is given by [6]

$$\kappa_i = K_2(\nu_i^*, \varepsilon) \cdot N \varepsilon^{1/2} \rho_{i\theta}^2 / \tau_i \quad , \tag{2.12}$$

with $\varepsilon = r/R$; the quantities ν_i^*, $\rho_{i\theta}$ and τ_i have their usual meaning and are defined in ref. [6]. Furthermore [6],

$$K_2 = K_{20} \cdot \left\{ \frac{1}{1 + a_2 \sqrt{\nu_i^*} + b_2 \nu_i^*} + \frac{c_2^2 \nu_i^* \varepsilon^3}{b_2 (1 + c_2 \nu_i^* \varepsilon^{3/2})} \right\} \quad , \tag{2.13}$$

with

$$\left.\begin{aligned} K_{20} &= 0.66 \\ a_2 &= 1.03 \\ b_2 &= 0.31 \\ c_2 &= 0.74 \end{aligned}\right\} \tag{2.14}$$

These neoclassical formulas are in cgs units. In the evaluation, $r_T = a/2$ was used. For tokamaks with noncircular cross-sections the minor radius a in eq. (2.11) is again replaced by $\bar{a}_{DP}$ of eq. (2.10), and $r_T = \bar{a}_{DP}/2$ is used. On the other hand, the value $\varepsilon = a_H/(2R)$ was used, by analogy with eq. (2.8) for δ_o and with the above definition of the aspect ratio A.

3. Discussion of the Results

The machine parameters of the six tokamaks ASDEX, INTOR, JET, PLT, TFTR and ZEPHYR are listed in Tabs. I to VI. Figures 1 to 36 then present the total energy confinement times $\tau_E^{TOT}(T)$, T = temperature, for the six tokamaks and, as dotted lines, the functions $\tau_E^{SW}(T)$, $\tau_E^{DP}(T)$, and $\tau_E^{NC}(T)$, as far as they fit within the chosen frames. Let us first discuss the temperature dependence of τ_E^{SW}, τ_E^{DP} and τ_E^{NC}. The trapped-ion τ_E, τ_E^{SW}, is infinite for low temperatures, decreases with medium temperatures and increases again with high temperatures. The anomalous electron τ_E, τ_E^{DP}, always increases with temperature. The neoclassical τ_E, τ_E^{NC}, varies little with temperature. Contrary to its dependence on density, $\tau_E^{NC}(T)$ exhibits a minimum in the plateau regime; this is a consequence of the interpolation formula chosen by the authors of ref. [6]. Another interpolation formula, chosen by Düchs et al. [10], yields somewhat smaller values of τ_E^{NC} at lower temperatures, but also exhibits a minimum when varying T. According to the different scalings of τ_E^{SW}, τ_E^{DP}, and τ_E^{NC} (see eq. (2.9) and ref. [1]) a variety of qualitatively and quantitatively different $\tau_E(T)$ curves is produced for different densities and machine parameters. It is seen that it would be misleading to simply put $\tau_E = \tau_E^{DP}$, as is sometimes done. Deviations from anomalous electron energy transport are brought about by neoclassical effects (at high densities) as well as by trapped-particle effects, i.e. by the dissipative trapped-ion instability. The step visible in the $\tau_E^{TOT}(T)$ curves indicates the onset of the dissipative trapped-ion instability, with the consequence of finite values of τ_E^{SW} for temperatures higher than the onset temperature. One should also note that $\tau_E^{SW} \propto (r_n/a)^3$ in the medium temperature region. Hence a knowledge of the density profile is rather important in order to determine τ_E^{TOT}. In order to show the influence of varying (r_n/a), the evaluation was made for two values, i.e. $r_n/\bar{a}_{sw} = 0.5$ (triangular density profile) and $r_n/\bar{a}_{sw} = 1.0$ (trapezoidal profile).

The more pessimistic cases, with $r_n/a = 0.5$, are discussed first. It is seen that at lower densities two temperature regimes exist;

at low temperatures τ_E^{TOT} is determined by τ_E^{DP} (anomalous-electron regime) and at high temperatures by τ_E^{SW} (trapped-ion regime). At higher densities there is also an intermediate temperature regime with τ_E^{TOT} determined by τ_E^{NC} (neoclassical regime). In particular, the trapped-ion τ_E, τ_E^{SW}, is predominant

for $T \gtrsim$ 3 to 4 keV in the case of ASDEX,

for $T \gtrsim$ 8 to 13 keV in the case of INTOR,

for $T \gtrsim$ 5 keV in the case of JET,

for $T \gtrsim$ 3.5 keV in the case of PLT,

for $T \gtrsim$ 6 keV in the case of TFTR,

for $T \gtrsim$ 7 to 10 keV in the case of ZEPHYR,

depending on the density. These numbers hold, of course, only within the density regime considered. Neoclassical transport is seen to matter in the following cases of those considered:

ASDEX, $N = 10^{14}$ cm^{-3},

INTOR, $N = 2 \times 10^{14}$ cm^{-3},

ZEPHYR, $N = 10^{15}$ cm^{-3}.

In many cases the effect of the anomalous trapped-particle transport upon τ_E^{TOT} is quite dramatic when $r_n/a = 0.5$ is assumed.

The trapped-particle transport is less important, however, in the other cases considered, viz. with $r_n/a = 1.0$. In these cases the general remarks of the preceding paragraph remain true, but, as mentioned, the impact of the anomalous trapped-ion transport is now less severe. This is best seen by looking at Figs. 1 to 36, but one may also note that τ_E^{SW} is now only predominant

for $T \gtrsim$ 5.5 to 8 keV in the case of ASDEX,

for $T \gtrsim$ 12.5 to 22 keV in the case of INTOR,

for $T \gtrsim$ 8 keV in the case of JET,

for $T \gtrsim$ 5 to 6.5 keV in the case of PLT,

for $T \gtrsim$ 10 keV in the case of TFTR,

for $T \gtrsim$ 12 to 18 keV in the case of ZEPHYR,

depending on the density.

Finally, a few remarks on the reliability of the results are added. In fact, the theories of all three transport mechanisms considered have their specific shortcomings. The theory of trapped-particle transport [1,2] is only based on an approximate, fluid theory [8] with the addition of strong Landau damping at mode-rational surfaces [7,11], but without consideration of other particle effects. On the other hand, the evaluation of these equations by numerical and analytical methods [1,2] seems quite accurate and reliable. At present, nonlinear microscopic transport theories cannot be carried through, and the estimate $D \sim \gamma/K_\perp^2$ should not be used after its invalidity has been demonstrated in the case of trapped-particle fluid theory [1]. It follows that eqs.(2.2) to (2.6) represent the best estimate for trapped-particle transport now available; but the error involved in this estimate is, of course, not now known.

In the case of anomalous electron energy transport, eq. (2.9) is not the result of a physical theory, but of a regression analysis of experimental results. However, the result of this analysis alone is not unique because internal relations between parameters exist owing to ohmic heating (and, possibly, for other reasons). The T-dependence of τ_E^{DP} is then taken from only one experiment [9] without knowing whether this result should be generalized to all other tokamak experiments. Moreover, owing to the empirical and statistical method used, no information exists on the regime of validity of eq. (2.9). A further ambiguity arises in that eq. (2.9) does not distinguish between global parameters, like the minor radius a, and local parameters like the scale lengths r_n and r_T

of the radial density and temperature profiles [5].

Even in the case of neoclassical transport there are at least two causes of possible inaccuracies regarding eqs. (2.11) to (2.14). Firstly, neoclassical transport has only been calculated for $\varepsilon \equiv r/R \ll 1$; when applied to cases with, for example, $\varepsilon \sim 0.2$, the inaccuracy of the theory is not known. Secondly, practical formulas for neoclassical transport are based on interpolation [6,10]. These interpolations can differ by, for example, factors of 2; moreover, the interpolations used seem to be ad hoc. That is to say, there is no discussion of how to interpolate in a multidimensional parameter space so that the interpolation chosen can be considered reasonable or even optimal. Nevertheless, the inaccuracies of the neoclassical transport theory may, perhaps, be less severe than those of the other theories.

It should be mentioned that the theory of trapped-particle anomalous transport [1,2] is in agreement with the results of the PLT heating experiment [12], where no such transport has been found so far. In ref. [12] maximal ion temperatures of 6 keV and 7.1 keV (on the magnetic axis) and average densities between 1.5×10^{13} and 3×10^{13} cm^{-3} are reported, together with maximal electron temperatures of 2.2 keV. Let us consider the following example: $T_{i,max} = 6$ keV, $T_{e,max} = 2.2$ keV, $N_{av} = 2 \times 10^{13}$ cm^{-3}. Then we may choose $T_{i,av} = 3$ keV, $T_{e,av} = 1.1$ keV, and the harmonic mean temperature T of eq. (2.6) becomes T = 1.6 keV. For these parameter values the above formulas, corrected for $T_i \neq T_e$, give

$$\tau_E^{SW} = 4.5 \text{ sec (or larger)},$$
$$\tau_E^{NC} = 2.0 \text{ sec},$$
$$\tau_E^{DP} = 0.14 \text{ sec}.$$

For τ_E^{NC} and τ_E^{DP} the corrections for $T_i \neq T_e$ include those caused by the modified expression for the energy density, viz. $E = \frac{3}{2} N (T_i + T_e)$,

while this correction drops out in the case of τ_E^{SW} owing to the convective and ambipolar character of this transport mechanism. It is seen that the anomalous trapped-particle energy transport is smaller than the neoclassical energy transport. Therefore it is clear that, according to the theory, anomalous trapped-particle transport was undetectable in the PLT heating experiment.

Acknowledgement

I thank D. Düchs and D. Pfirsch for making available and discussing with me their results on anomalous electron energy transport prior to publication. The τ_E (T) plots of Figs. 1 to 36 were programmed by M. Richter-Glötzl; her very useful assistance is gratefully acknowledged. I also thank F. Sardei for reading the manuscript.

References

[1] F. Sardei and H.K. Wimmel, Improved Formulas for Trapped-Ion Anomalous Transport in Tokamaks without and with Shear, Report IPP 6/196 (March 1980, Max-Planck-Institut für Plasmaphysik, Garching).

[2] F. Sardei and H.K. Wimmel, New Scaling Laws for Trapped-Particle Anomalous Transport in Tokamaks, Report IPP 6/197 (April 1980, Max-Planck-Institut für Plasmaphysik, Garching).

[3] D. Düchs, D. Pfirsch, H. Ringler, H. Wobig, Skalierungsgesetze für den Elektronenenergietransport in toroidalen Plasmen, Verhandlungen DPG (1980), p. 746.

[4] D. Düchs, D. Pfirsch, A. Schlüter, Scaling of Energy Confinement Time: Error Estimates and Dependence on Plasma Temperature, Sherwood Meeting, Tucson, Ariz. (1980).

[5] D. Düchs, D. Pfirsch, A. Schlüter, Scaling of Electron Energy Confinement Time τ_{Ee}: Error Estimates (and Dependence on Plasma Temperature), Workshop on Optimization of Toroidal Confinement, Hiroshima (1980).

[6] F.L. Hinton and R.D. Hazeltine, Revs. of Mod. Phys. 48, 239-308 (1976).

[7] F. Sardei and H.K. Wimmel, Nucl. Fusion 19, 1635 - 1641 (1979).

[8] B.B. Kadomtsev and O.P. Pogutse, in Reviews of Plasma Physics (M.A. Leontovich, Ed.) Vol. 5, pp. 379 - 383 (Consultants Bureau, New York, 1970).

[9] Cited in: J.D. Callen et al., INTOR internal report No. 2, Energy and Particle Confinement, 2nd Meeting of the INTOR Workshop (IAEA, Vienna, 1979) p.4, Fig. 1-1.

[10] D. Düchs, D.E. Post, P.H. Rutherford, Nucl. Fusion 17, 565 - 609 (1977).

[11] N.T. Gladd and D.W. Ross, Phys. Fluids 16, 1706 - 1718 (1973).

[12] W. Stodiek et al., Transport Studies in the Princeton Large Torus, 8th Int. Conf. on Plasma Physics and Contr. Nucl. Fus. Res., Paper IAEA-CN-38/A-1, Brussels, 1980.

List of Tables* (p. 13 to 15)

---

*Note: The quantities $\bar{a}_{SW}$ and $\bar{a}_{DP}$ are designated as

"AVER. MINOR RADIUS-SW (CM)"

and

"AVER. MINOR RADIUS-P (CM)"

in Tables I to VI.

Table I

PARAMETERS FOR A S D E X

HORIZ. MINOR RADIUS (CM)	=	4.ØØE+Ø1	
VERTIC. MINOR RADIUS (CM)	=	4.ØØE+Ø1	
AVER. MINOR RADIUS-SW(CM)	=	4.ØØE+Ø1	
AVER. MINOR RADIUS-P(CM)	=	4.ØØE+Ø1	
Q SCALE RQ (CM)	=	3.2ØE+Ø1	
MAJOR RADIUS (CM)	=	1.54E+Ø2	
ASPECT RATIO R/AH	=	3.85E+ØØ	
SAFETY FACTOR Q	=	2.ØØE+ØØ	AT HALF AVERAGE MINOR RADIUS
SAFETY FACTOR QA	=	3.ØØE+ØØ	AT AVERAGE MINOR RADIUS
DELTA-NOUGHT	=	3.6ØE-Ø1	
TOROID. B FIELD (GAUSS)	=	3.ØØE+Ø4	
ION MASS (GRAMM)	=	3.35E-24	
ALPHA = MCRIT/MMARG	=	4.ØØE+ØØ	
ATOMIC WEIGHT	=	2.ØØE+ØØ	
RATIO NYI/NYE	=	1.17E-Ø2	
EFFECTIVE Z	=	1.ØØE+ØØ	

Table II

PARAMETERS FOR I N T O R

HORIZ. MINOR RADIUS (CM)	=	1.2ØE+Ø2	
VERTIC. MINOR RADIUS (CM)	=	1.8ØE+Ø2	
AVER. MINOR RADIUS-SW(CM)	=	1.36E+Ø2	
AVER. MINOR RADIUS-P(CM)	=	1.41E+Ø2	
Q SCALE RQ (CM)	=	1.Ø9E+Ø2	
MAJOR RADIUS (CM)	=	4.8ØE+Ø2	
ASPECT RATIO R/AH	=	4.ØØE+ØØ	
SAFETY FACTOR Q	=	2.ØØE+ØØ	AT HALF AVERAGE MINOR RADIUS
SAFETY FACTOR QA	=	3.ØØE+ØØ	AT AVERAGE MINOR RADIUS
DELTA-NOUGHT	=	3.54E-Ø1	
TOROID. B FIELD (GAUSS)	=	5.ØØE+Ø4	
ION MASS (GRAMM)	=	3.35E-24	
ALPHA = MCRIT/MMARG	=	4.ØØE+ØØ	
ATOMIC WEIGHT	=	2.ØØE+ØØ	
RATIO NYI/NYE	=	1.17E-Ø2	
EFFECTIVE Z	=	1.ØØE+ØØ	

Table III

PARAMETERS FOR J E T

HORIZ. MINOR RADIUS (CM)	=	1.25E+Ø2	
VERTIC. MINOR RADIUS (CM)	=	2.1ØE+Ø2	
AVER. MINOR RADIUS-SW(CM)	=	1.44E+Ø2	
AVER. MINOR RADIUS-P(CM)	=	1.52E+Ø2	
Q SCALE RQ (CM)	=	1.15E+Ø2	
MAJOR RADIUS (CM)	=	2.96E+Ø2	
ASPECT RATIO R/AH	=	2.37E+ØØ	
SAFETY FACTOR Q	=	2.ØØE+ØØ	AT HALF AVERAGE MINOR RADIUS
SAFETY FACTOR QA	=	3.ØØE+ØØ	AT AVERAGE MINOR RADIUS
DELTA-NOUGHT	=	4.6ØE-Ø1	
TOROID. B FIELD (GAUSS)	=	3.4ØE+Ø4	
ION MASS (GRAMM)	=	3.35E-24	
ALPHA = MCRIT/MMARG	=	4.ØØE+ØØ	
ATOMIC WEIGHT	=	2.ØØE+ØØ	
RATIO NYI/NYE	=	1.17E-Ø2	
EFFECTIVE Z	=	1.ØØE+ØØ	

Table IV

PARAMETERS FOR P L T

HORIZ. MINOR RADIUS (CM)	=	4.ØØE+Ø1	
VERTIC. MINOR RADIUS (CM)	=	4.ØØE+Ø1	
AVER. MINOR RADIUS-SW(CM)	=	4.ØØE+Ø1	
AVER. MINOR RADIUS-P(CM)	=	4.ØØE+Ø1	
Q SCALE RQ (CM)	=	3.2ØE+Ø1	
MAJOR RADIUS (CM)	=	1.3ØE+Ø2	
ASPECT RATIO R/AH	=	3.25E+ØØ	
SAFETY FACTOR Q	=	2.ØØE+ØØ	AT HALF AVERAGE MINOR RADIUS
SAFETY FACTOR QA	=	3.ØØE+ØØ	AT AVERAGE MINOR RADIUS
DELTA-NOUGHT	=	3.92E-Ø1	
TOROID. B FIELD (GAUSS)	=	3.2ØE+Ø4	
ION MASS (GRAMM)	=	3.35E-24	
ALPHA = MCRIT/MMARG	=	4.ØØE+ØØ	
ATOMIC WEIGHT	=	2.ØØE+ØØ	
RATIO NYI/NYE	=	1.17E-Ø2	
EFFECTIVE Z	=	1.ØØE+ØØ	

Table V

PARAMETERS FOR T F T R

HORIZ. MINOR RADIUS (CM)	=	8.5ØE+Ø1	
VERTIC. MINOR RADIUS (CM)	=	8.5ØE+Ø1	
AVER. MINOR RADIUS-SW(CM)	=	8.5ØE+Ø1	
AVER. MINOR RADIUS-P(CM)	=	8.5ØE+Ø1	
Q SCALE RQ (CM)	=	6.8ØE+Ø1	
MAJOR RADIUS (CM)	=	2.48E+Ø2	
ASPECT RATIO R/AH	=	2.92E+ØØ	
SAFETY FACTOR Q	=	2.ØØE+ØØ	AT HALF AVERAGE MINOR RADIUS
SAFETY FACTOR QA	=	3.ØØE+ØØ	AT AVERAGE MINOR RADIUS
DELTA-NOUGHT	=	4.14E-Ø1	
TOROID. B FIELD (GAUSS)	=	5.6ØE+Ø4	
ION MASS (GRAMM)	=	3.35E-24	
ALPHA = MCRIT/MMARG	=	4.ØØE+ØØ	
ATOMIC WEIGHT	=	2.ØØE+ØØ	
RATIO NYI/NYE	=	1.17E-Ø2	
EFFECTIVE Z	=	1.ØØE+ØØ	

Table VI

PARAMETERS FOR Z E P H Y R

HORIZ. MINOR RADIUS (CM)	=	4.7ØE+Ø1	
VERTIC. MINOR RADIUS (CM)	=	4.7ØE+Ø1	
AVER. MINOR RADIUS-SW(CM)	=	4.7ØE+Ø1	
AVER. MINOR RADIUS-P(CM)	=	4.7ØE+Ø1	
Q SCALE RQ (CM)	=	3.76E+Ø1	
MAJOR RADIUS (CM)	=	1.26E+Ø2	
ASPECT RATIO R/AH	=	2.68E+ØØ	
SAFETY FACTOR Q	=	2.ØØE+ØØ	AT HALF AVERAGE MINOR RADIUS
SAFETY FACTOR QA	=	3.ØØE+ØØ	AT AVERAGE MINOR RADIUS
DELTA-NOUGHT	=	4.32E-Ø1	
TOROID. B FIELD (GAUSS)	=	9.7ØE+Ø4	
ION MASS (GRAMM)	=	3.35E-24	
ALPHA = MCRIT/MMARG	=	4.ØØE+ØØ	
ATOMIC WEIGHT	=	2.ØØE+ØØ	
RATIO NYI/NYE	=	1.17E-Ø2	
EFFECTIVE Z	=	1.ØØE+ØØ	

List of Figures

Figs. 1 to 6: τ_E^{TOT} (T) for ASDEX.

Average densities: N = 1.0×10^{13} ; 3.0×10^{13}; 1.0×10^{14} cm^{-3} .

Linear density profiles with r_n/a = 0.5 and 1.0,

$\eta \equiv d\ln T/d\ln N = 1$, $Z_{eff} = 1$.

Figs. 7 to 12: τ_E^{TOT} (T) for INTOR.

Average densities: N = 5.0×10^{13}; 1.0×10^{14}; 2.0×10^{14} cm^{-3} .

Figs. 13 to 18: τ_E^{TOT}(T) for JET.

Average densities: N = 2.5×10^{13}; 5.0×10^{13}; 1.0×10^{14} cm^{-3} .

Figs. 19 to 24: τ_E^{TOT}(T) for PLT.

Average densities: N = 2.0×10^{13}; 3.0×10^{13}; 1.0×10^{14} cm^{-3} .

Figs. 25 to 30: τ_E^{TOT}(T) for TFTR.

Average densities: N = 1.0×10^{13}; 3.0×10^{13}; 1.0×10^{14} cm^{-3} .

Figs. 31 to 36: τ_E^{TOT}(T) for ZEPHYR.

Average densities: N = 1.0×10^{14}; 3.0×10^{14}; 1.0×10^{15} cm^{-3} .

Fig. 1.

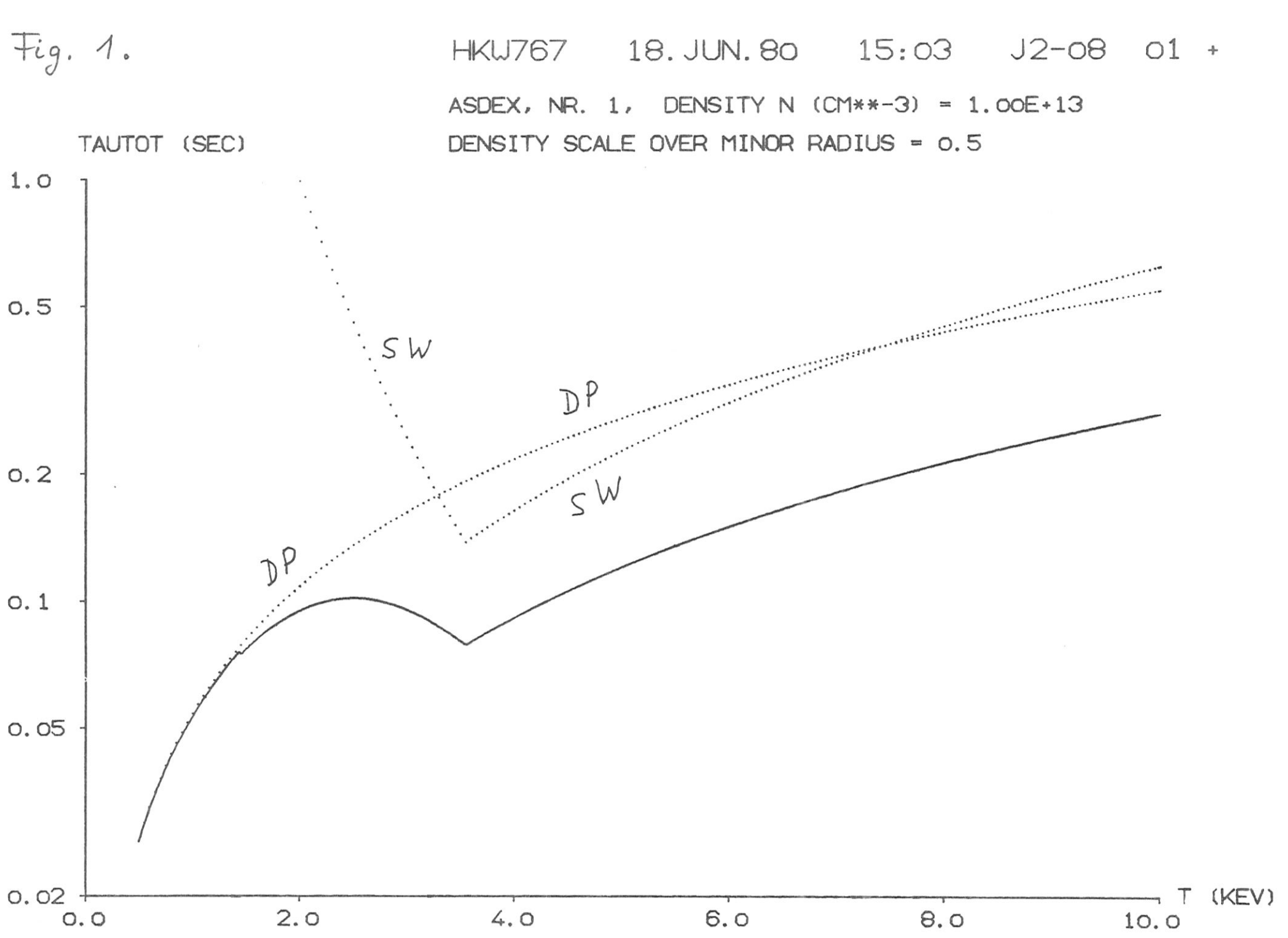
HKW767 18. JUN. 80 15:03 J2-08 01 +
ASDEX, NR. 1, DENSITY N (CM**-3) = 1.00E+13
DENSITY SCALE OVER MINOR RADIUS = 0.5
TAUTOT (SEC)
1.0
0.5
0.2
0.1
0.05
0.02
SW
DP
DP
SW
0.0
2.0
4.0
6.0
8.0
10.0
T (KEV)

Fig. 2.

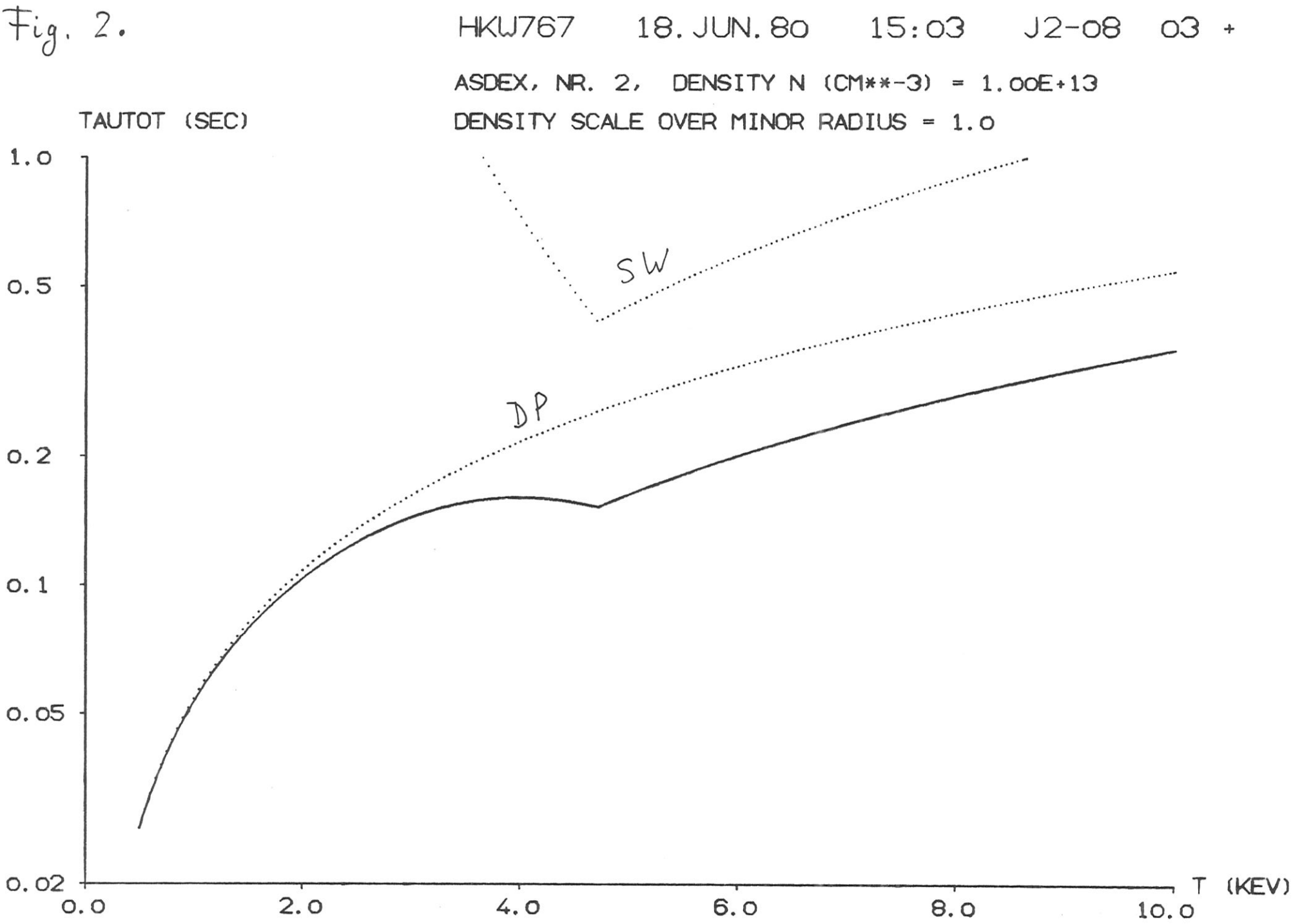
HKW767 18. JUN. 80 15:03 J2-08 03 +
ASDEX, NR. 2, DENSITY N (CM**-3) = 1.00E+13
DENSITY SCALE OVER MINOR RADIUS = 1.0
TAUTOT (SEC)
1.0
0.5
0.2
0.1
0.05
0.02
SW
DP
0.0
2.0
4.0
6.0
8.0
10.0
T (KEV)

Fig. 3.

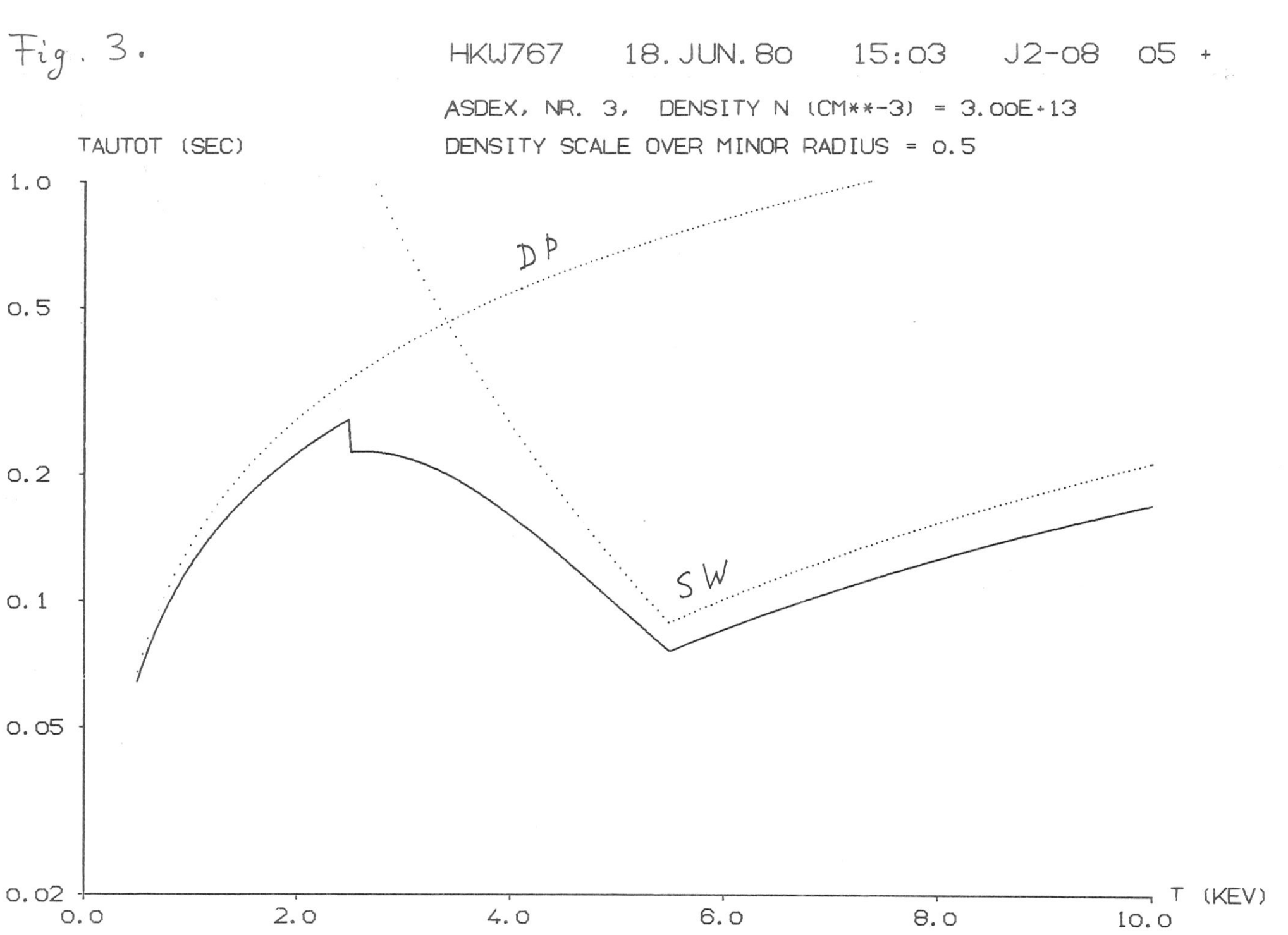
HKW767 18. JUN. 80 15:03 J2-08 05 +
ASDEX, NR. 3, DENSITY N (CM**-3) = 3.00E+13
DENSITY SCALE OVER MINOR RADIUS = 0.5
TAUTOT (SEC)
1.0
0.5
0.2
0.1
0.05
0.02
DP
SW
0.0
2.0
4.0
6.0
8.0
10.0
T (KEV)

Fig. 4.

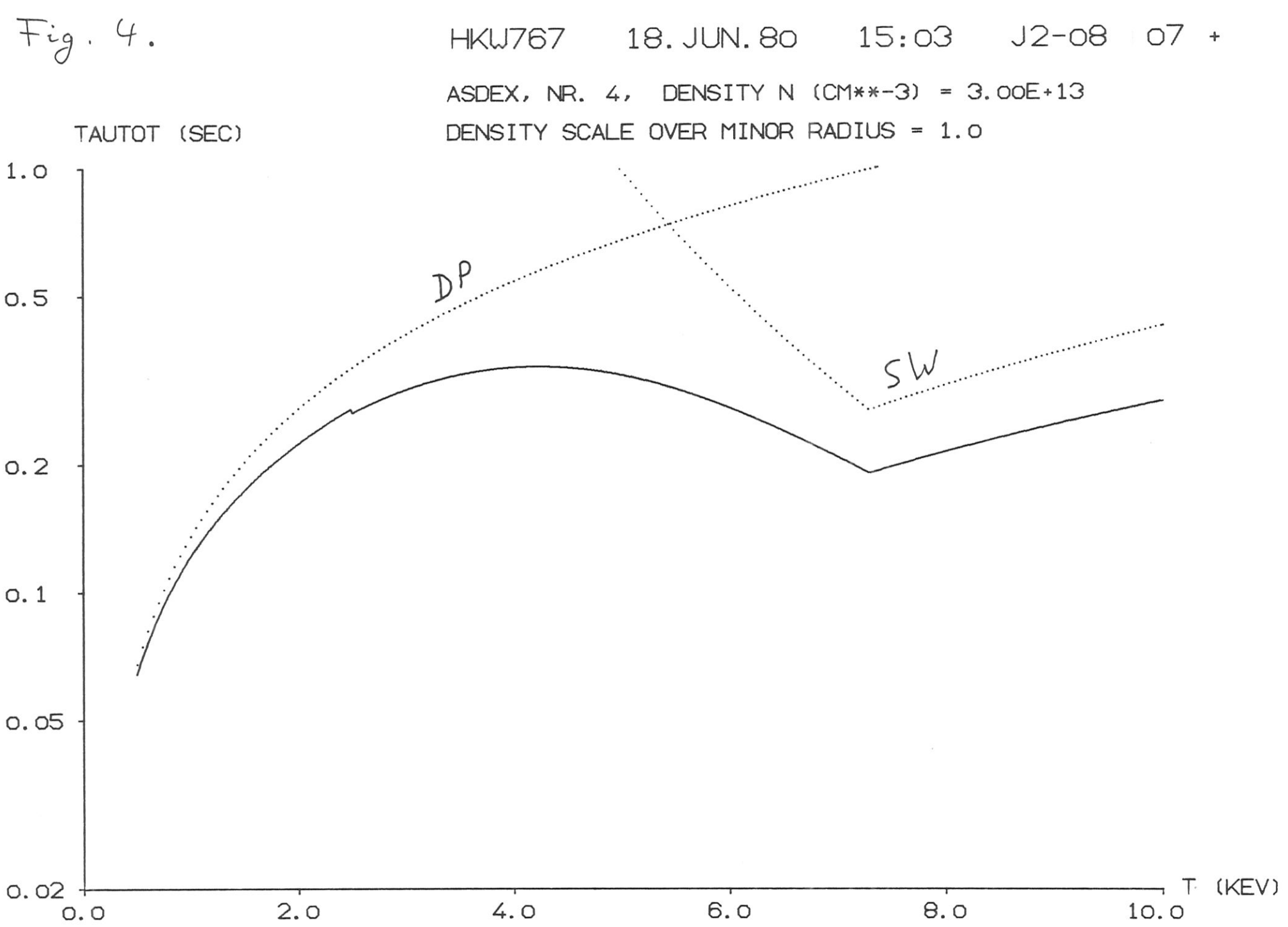
HKW767 18. JUN. 80 15:03 J2-08 07 +
ASDEX, NR. 4, DENSITY N (CM**-3) = 3.00E+13
DENSITY SCALE OVER MINOR RADIUS = 1.0
TAUTOT (SEC)
1.0
0.5
0.2
0.1
0.05
0.02
DP
SW
0.0
2.0
4.0
6.0
8.0
10.0
T (KEV)

Fig. 5.

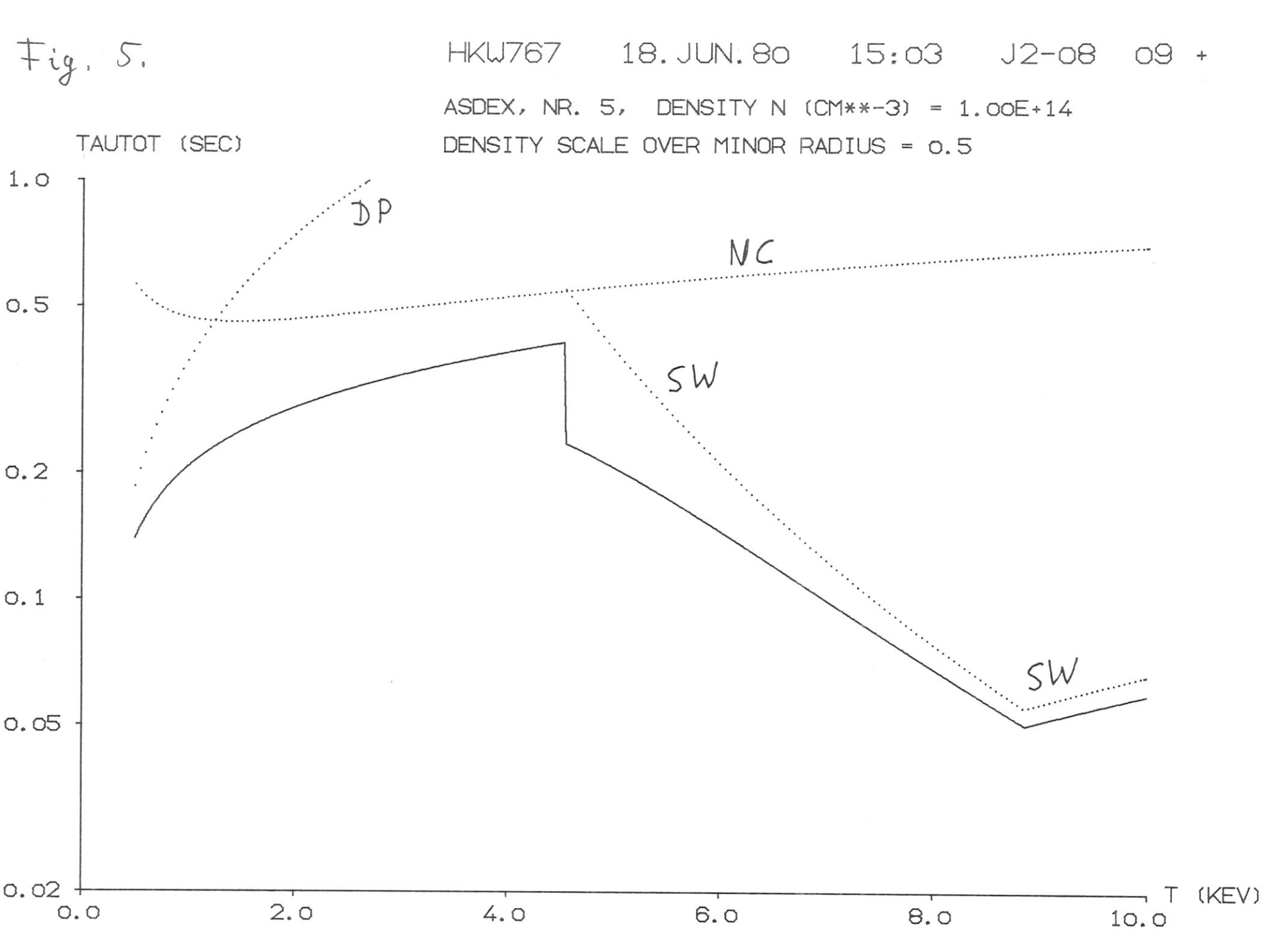
HKW767 18. JUN. 80 15:03 J2-08 09 +
ASDEX, NR. 5, DENSITY N (CM**-3) = 1.00E+14
DENSITY SCALE OVER MINOR RADIUS = 0.5
TAUTOT (SEC)
1.0
0.5
0.2
0.1
0.05
0.02
DP
NC
SW
SW
0.0
2.0
4.0
6.0
8.0
10.0
T (KEV)

Fig. 6.

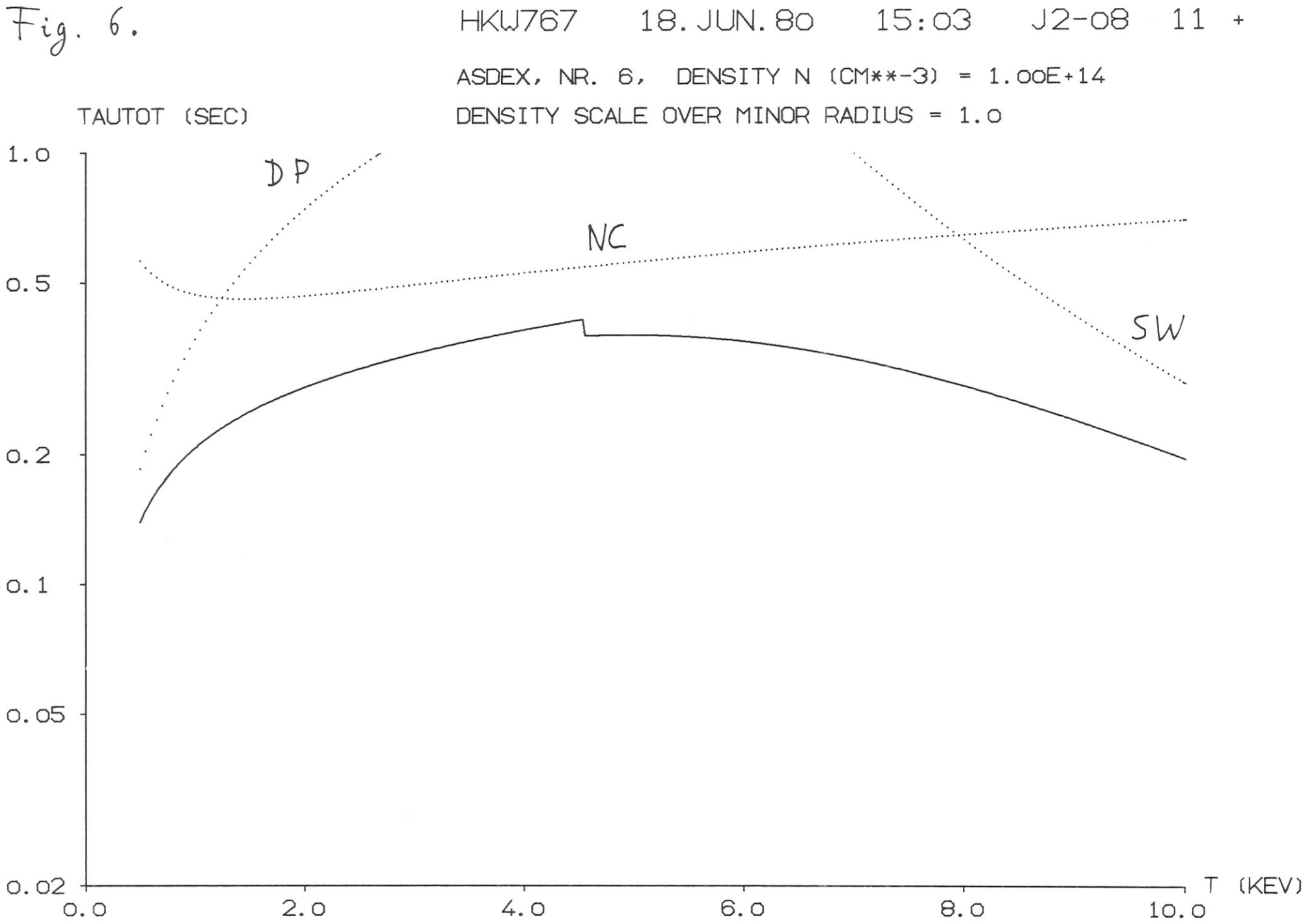
HKW767 18. JUN. 80 15:03 J2-08 11 +
ASDEX, NR. 6, DENSITY N (CM**-3) = 1.00E+14
DENSITY SCALE OVER MINOR RADIUS = 1.0
TAUTOT (SEC)
1.0
0.5
0.2
0.1
0.05
0.02
DP
NC
SW
0.0
2.0
4.0
6.0
8.0
10.0
T (KEV)

Fig. 7.

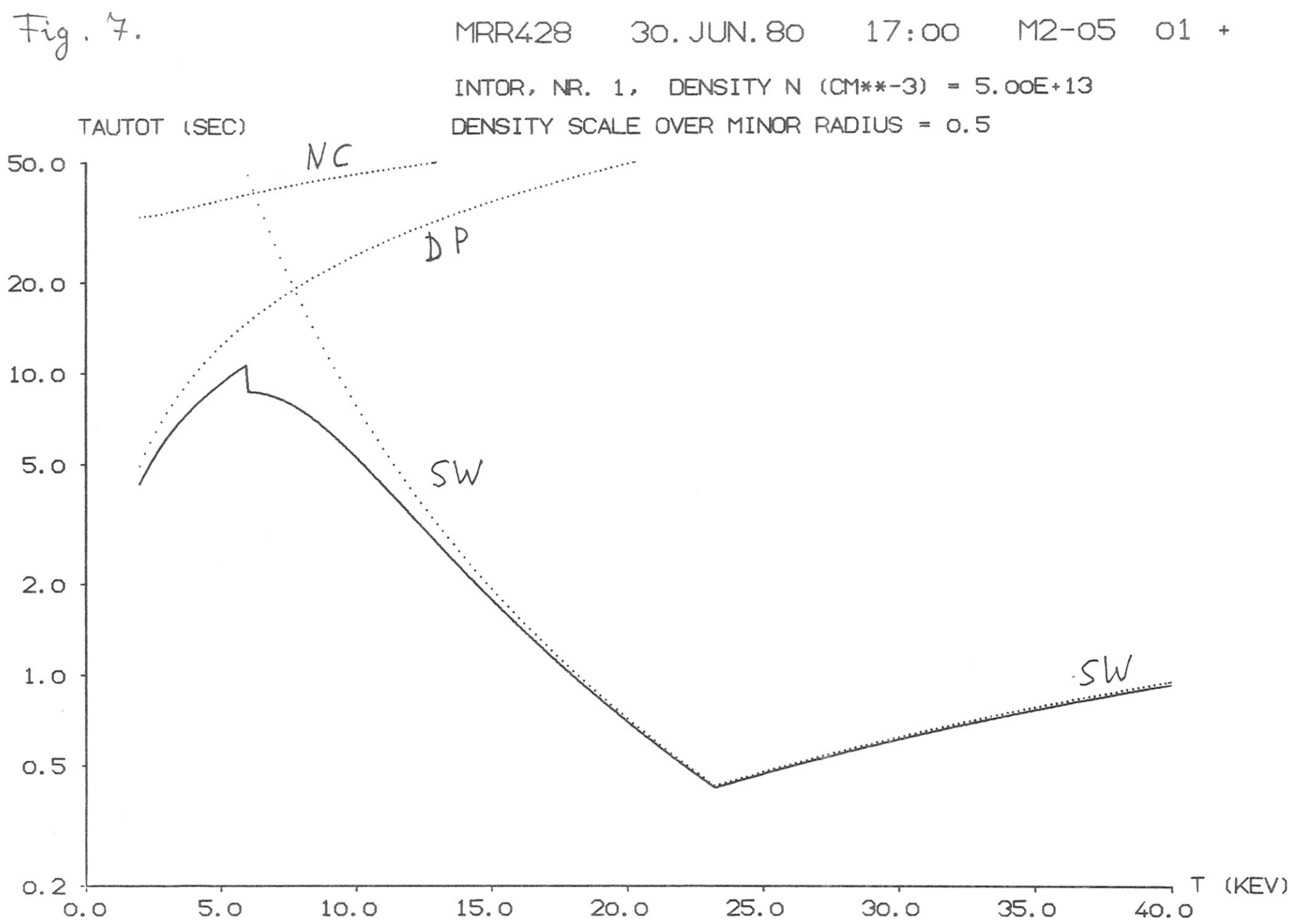
MRR428 30. JUN. 80 17:00 M2-05 01 +
INTOR, NR. 1, DENSITY N (CM**-3) = 5.00E+13
DENSITY SCALE OVER MINOR RADIUS = 0.5
TAUTOT (SEC)
NC
DP
SW
SW
50.0
20.0
10.0
5.0
2.0
1.0
0.5
0.2
0.0
5.0
10.0
15.0
20.0
25.0
30.0
35.0
40.0
T (KEV)

Fig. 8.

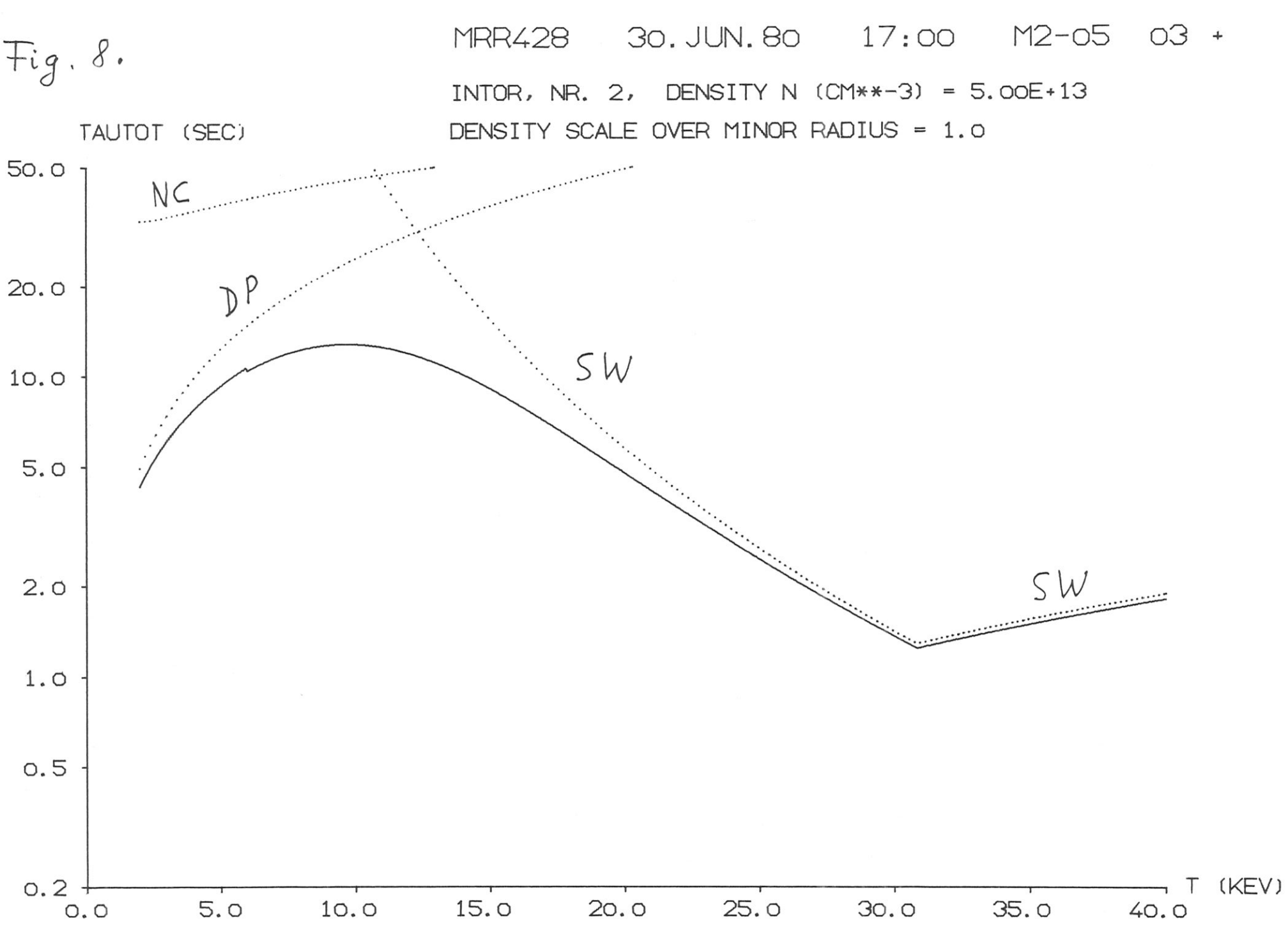
MRR428 30. JUN. 80 17:00 M2-05 03 +
INTOR, NR. 2, DENSITY N (CM**-3) = 5.00E+13
DENSITY SCALE OVER MINOR RADIUS = 1.0
TAUTOT (SEC)
50.0
20.0
10.0
5.0
2.0
1.0
0.5
0.2
NC
DP
SW
SW
0.0
5.0
10.0
15.0
20.0
25.0
30.0
35.0
40.0
T (KEV)

Fig. 9.

MRR428 30. JUN. 80 17:00 M2-05 05 +

INTOR, NR. 3, DENSITY N (CM**-3) = 1.00E+14

DENSITY SCALE OVER MINOR RADIUS = 0.5

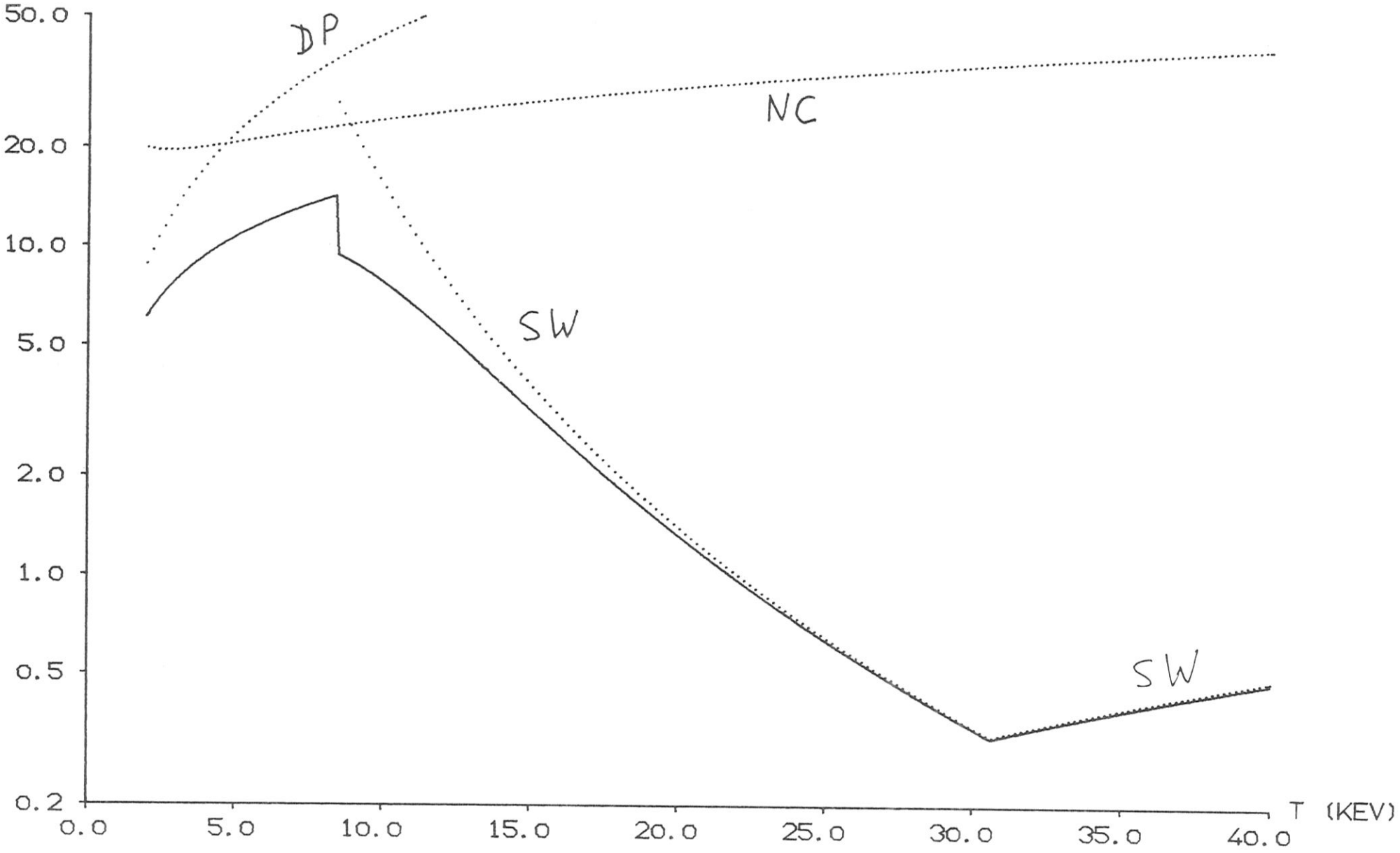

Fig. 10.

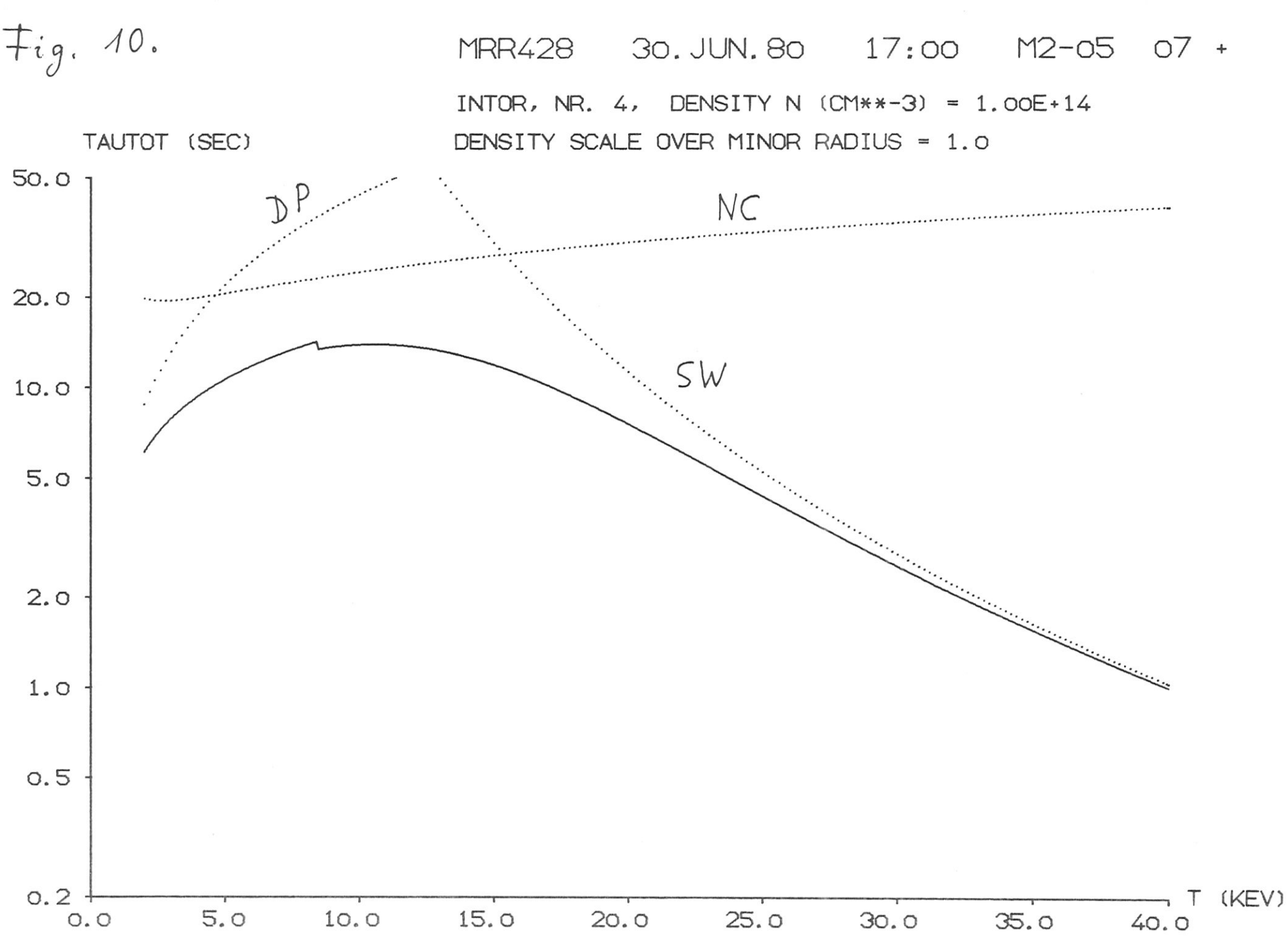
MRR428 30. JUN. 80 17:00 M2-05 07 +
INTOR, NR. 4, DENSITY N (CM**-3) = 1.00E+14
DENSITY SCALE OVER MINOR RADIUS = 1.0
TAUTOT (SEC)
50.0
20.0
10.0
5.0
2.0
1.0
0.5
0.2
DP
NC
SW
0.0
5.0
10.0
15.0
20.0
25.0
30.0
35.0
40.0
T (KEV)

Fig. 11.

MRR428 30. JUN. 80 17:00 M2-05 09 +

INTOR, NR. 5, DENSITY N (CM**-3) = 2.00E+14

DENSITY SCALE OVER MINOR RADIUS = 0.5

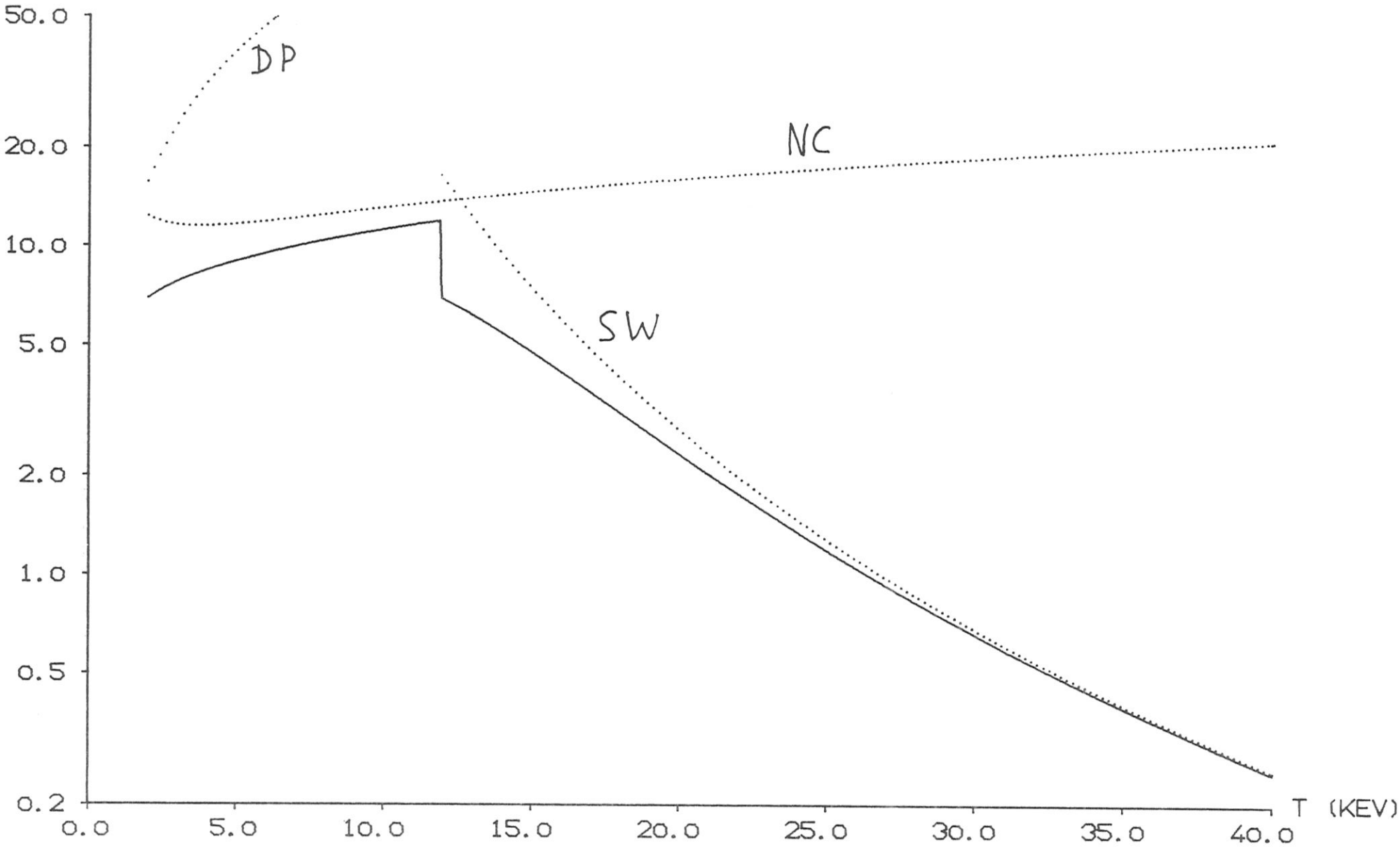

Fig. 12.

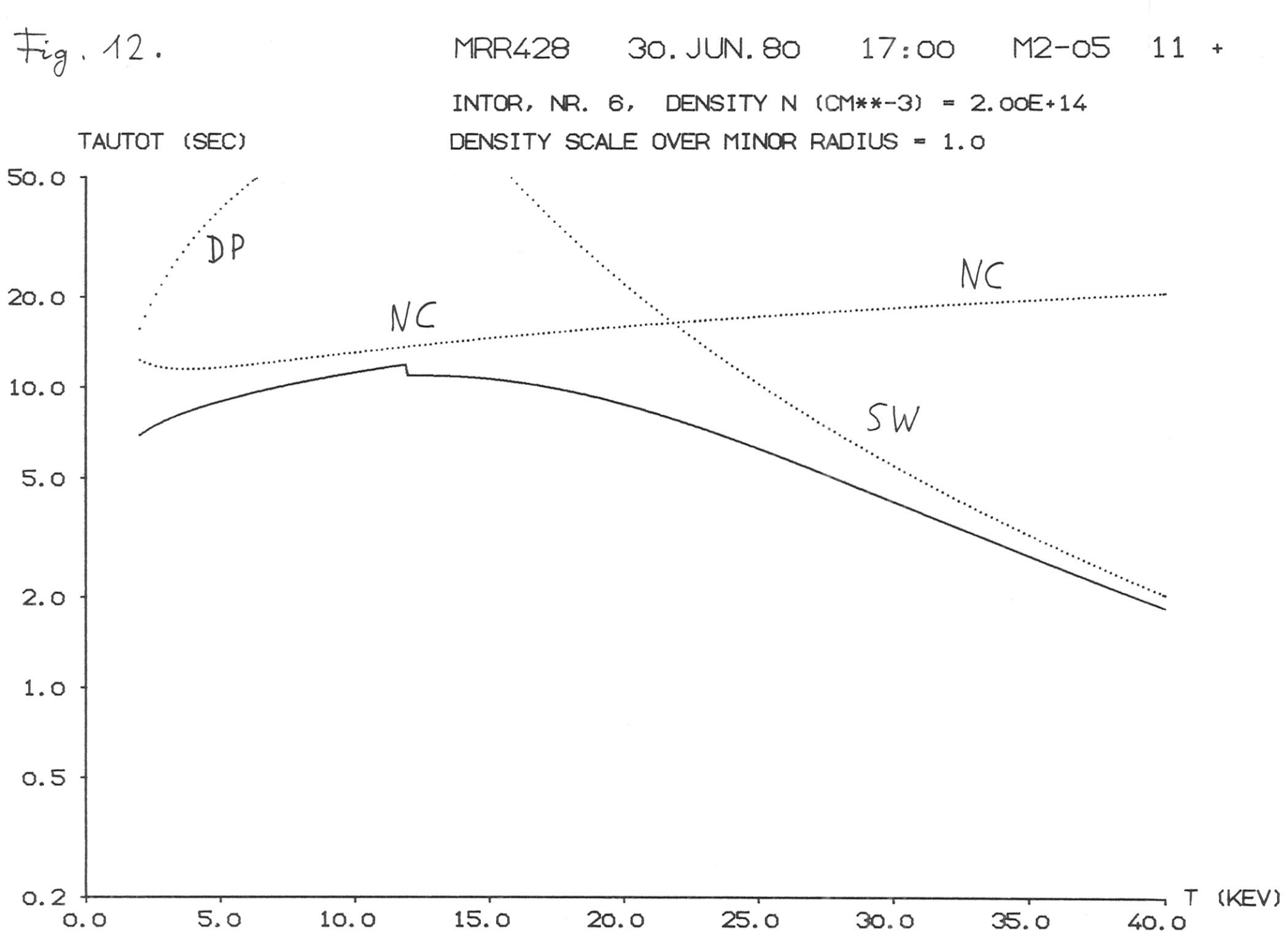
MRR428 30. JUN. 80 17:00 M2-05 11 +
INTOR, NR. 6, DENSITY N (CM**-3) = 2.00E+14
DENSITY SCALE OVER MINOR RADIUS = 1.0
TAUTOT (SEC)
50.0
20.0
10.0
5.0
2.0
1.0
0.5
0.2
DP
NC
NC
SW
0.0
5.0
10.0
15.0
20.0
25.0
30.0
35.0
40.0
T (KEV)

Fig. 13.

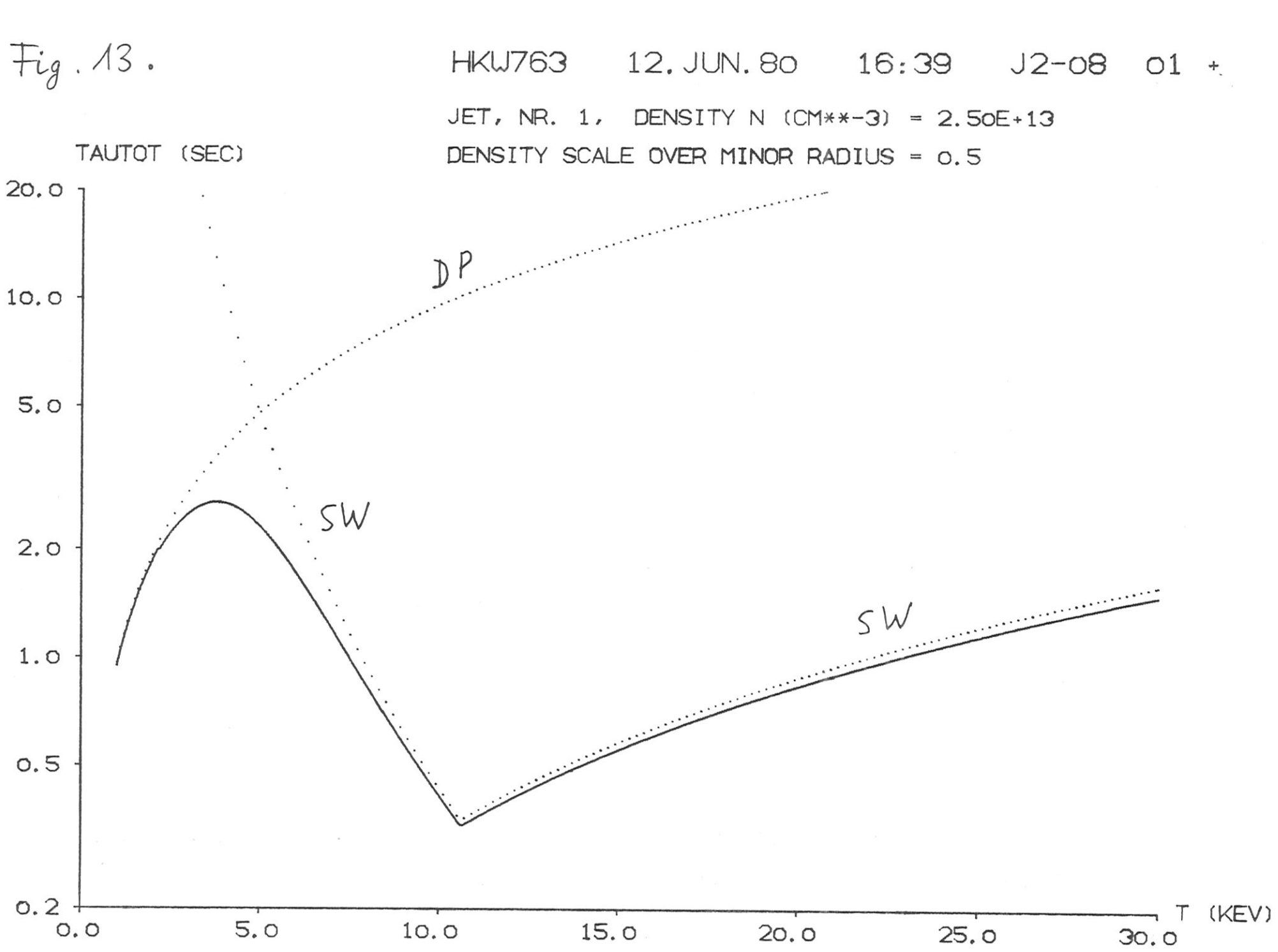
HKW763 12. JUN. 80 16:39 J2-08 01 +
JET, NR. 1, DENSITY N (CM**-3) = 2.50E+13
DENSITY SCALE OVER MINOR RADIUS = 0.5
TAUTOT (SEC)
20.0
10.0
5.0
2.0
1.0
0.5
0.2
DP
SW
SW
0.0
5.0
10.0
15.0
20.0
25.0
30.0
T (KEV)

Fig. 14.

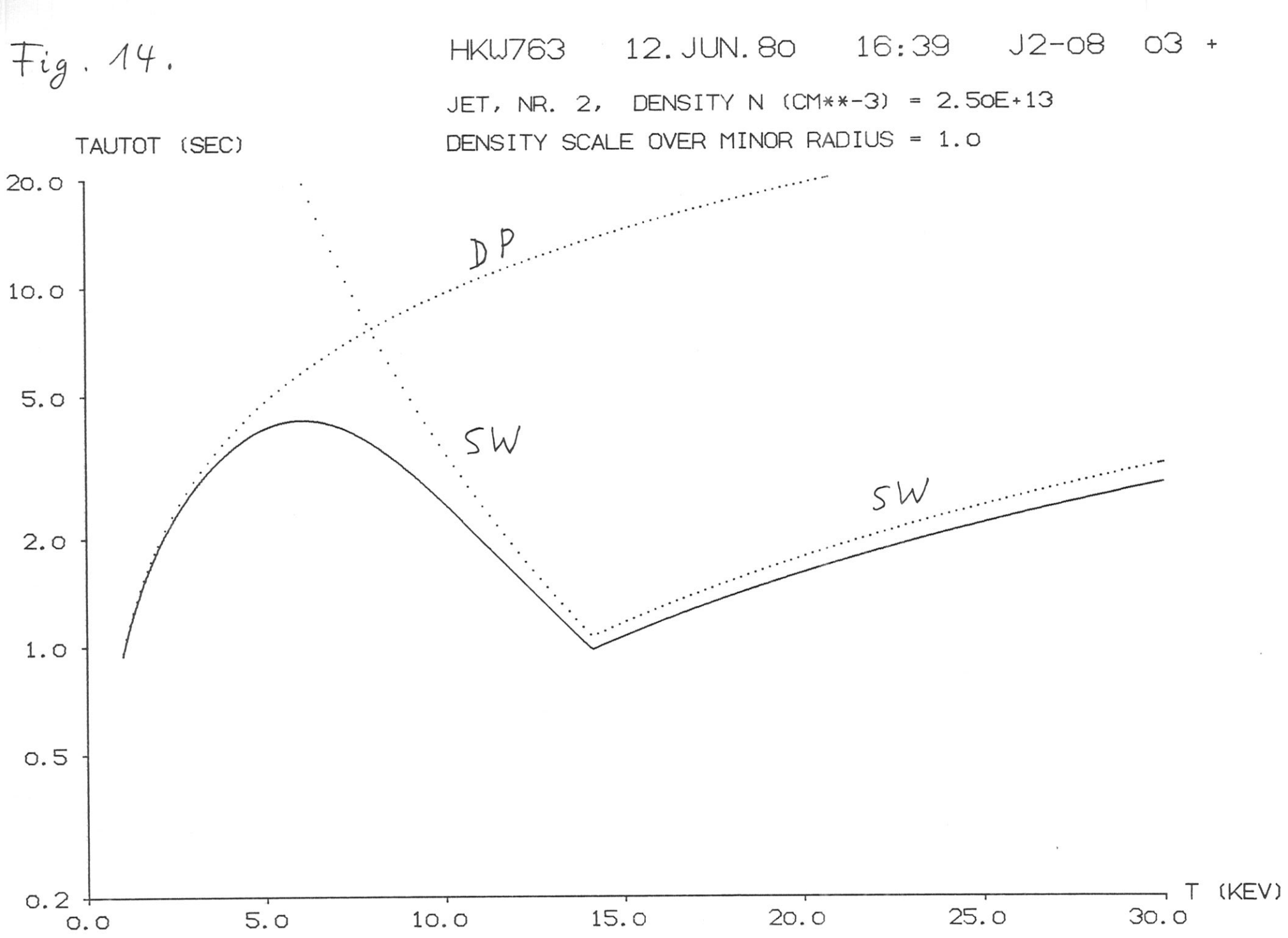
HKW763 12. JUN. 80 16:39 J2-08 03 +
JET, NR. 2, DENSITY N (CM**-3) = 2.50E+13
DENSITY SCALE OVER MINOR RADIUS = 1.0
TAUTOT (SEC)
20.0
10.0
5.0
2.0
1.0
0.5
0.2
DP
SW
SW
0.0
5.0
10.0
15.0
20.0
25.0
30.0
T (KEV)

Fig. 15.

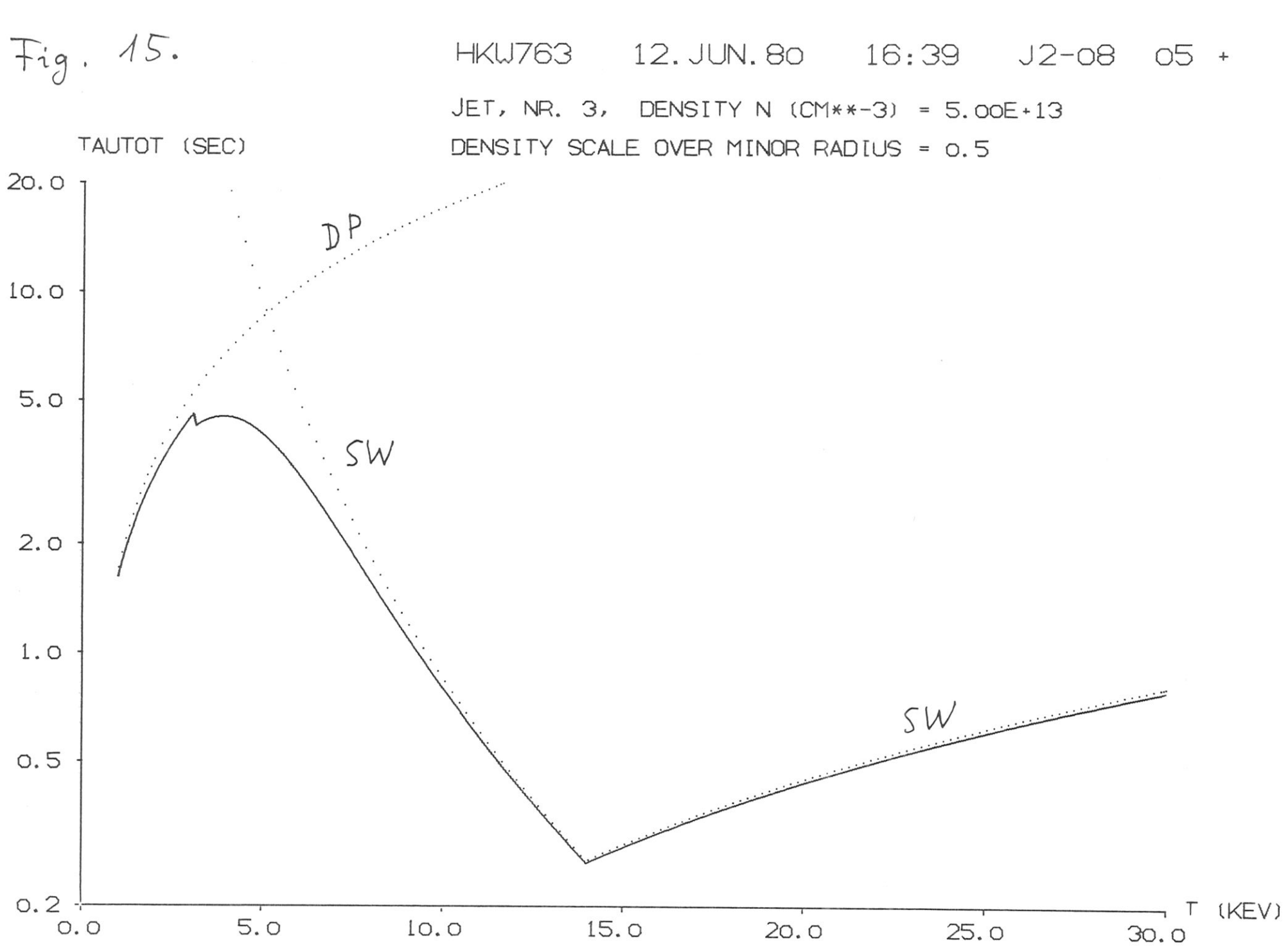
HKW763 12. JUN. 80 16:39 J2-08 05 +
JET, NR. 3, DENSITY N (CM**-3) = 5.00E+13
DENSITY SCALE OVER MINOR RADIUS = 0.5
TAUTOT (SEC)
20.0
10.0
5.0
2.0
1.0
0.5
0.2
DP
SW
SW
0.0
5.0
10.0
15.0
20.0
25.0
30.0
T (KEV)

Fig. 16.

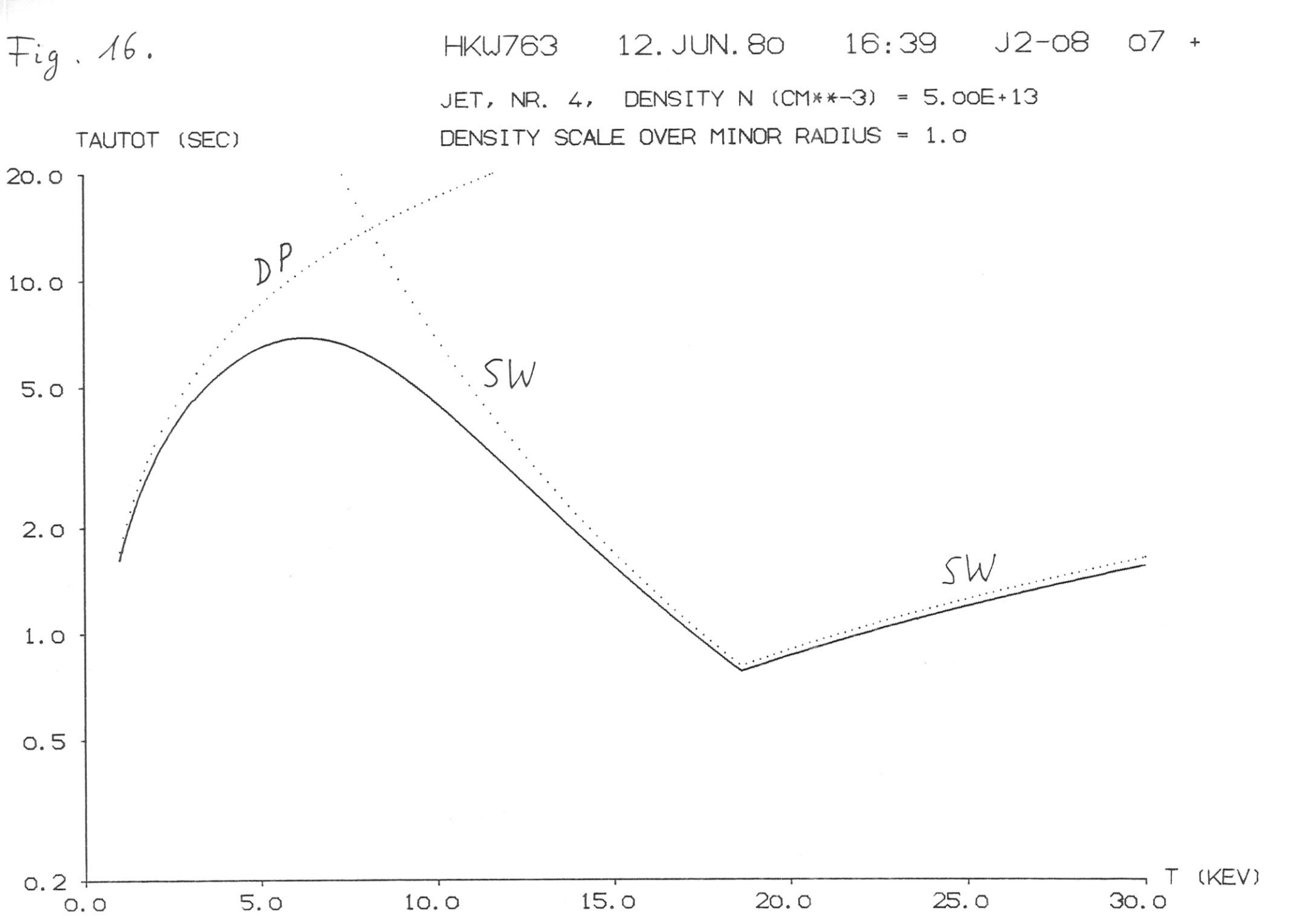
HKW763 12. JUN. 80 16:39 J2-08 07 +
JET, NR. 4, DENSITY N (CM**-3) = 5.00E+13
DENSITY SCALE OVER MINOR RADIUS = 1.0
TAUTOT (SEC)
20.0
10.0
5.0
2.0
1.0
0.5
0.2
DP
SW
SW
0.0
5.0
10.0
15.0
20.0
25.0
30.0
T (KEV)

Fig. 17.

HKW763 12. JUN. 80 16:39 J2-08 09 +

JET, NR. 5, DENSITY N (CM**-3) = 1.00E+14

DENSITY SCALE OVER MINOR RADIUS = 0.5

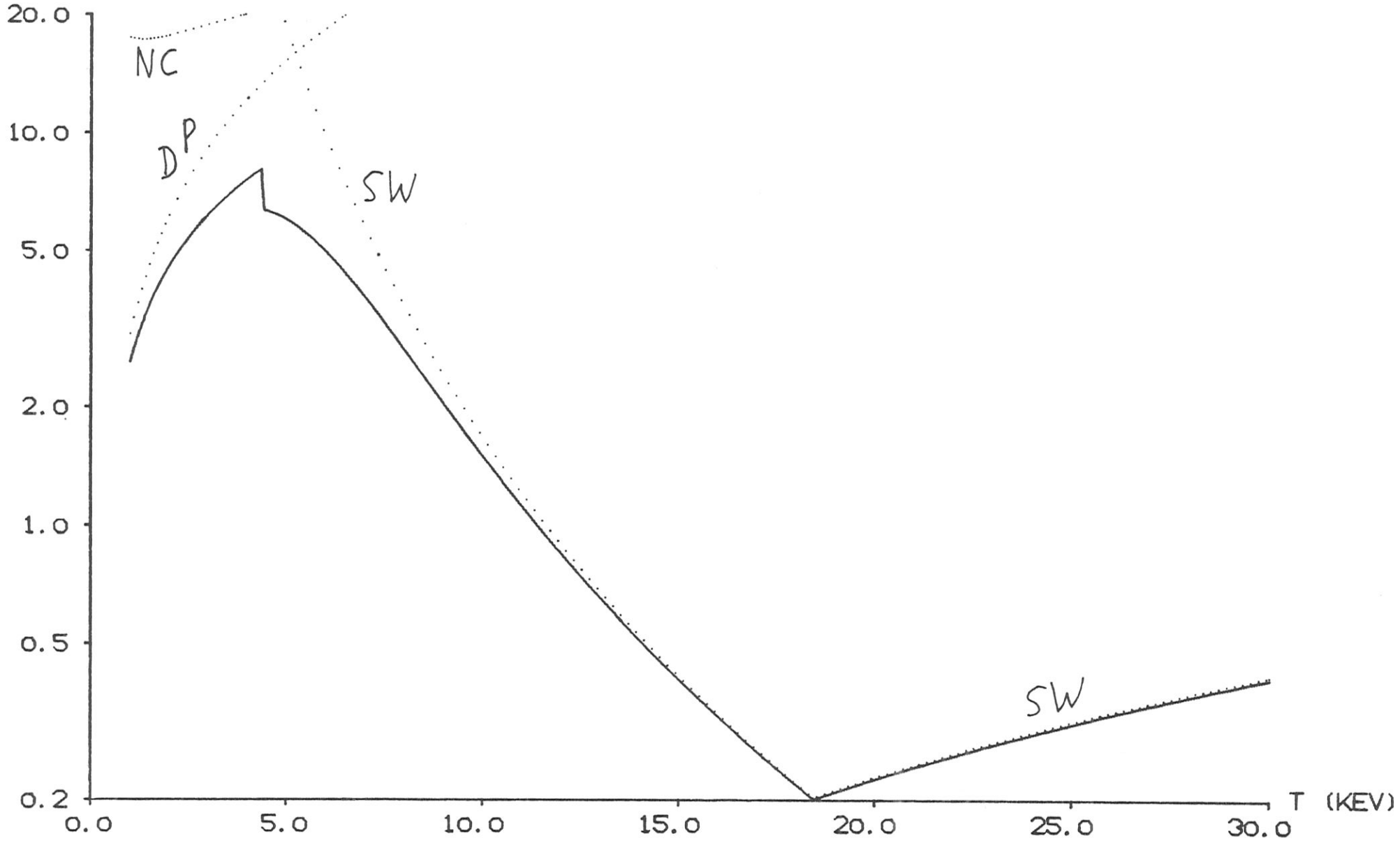

Fig. 18.

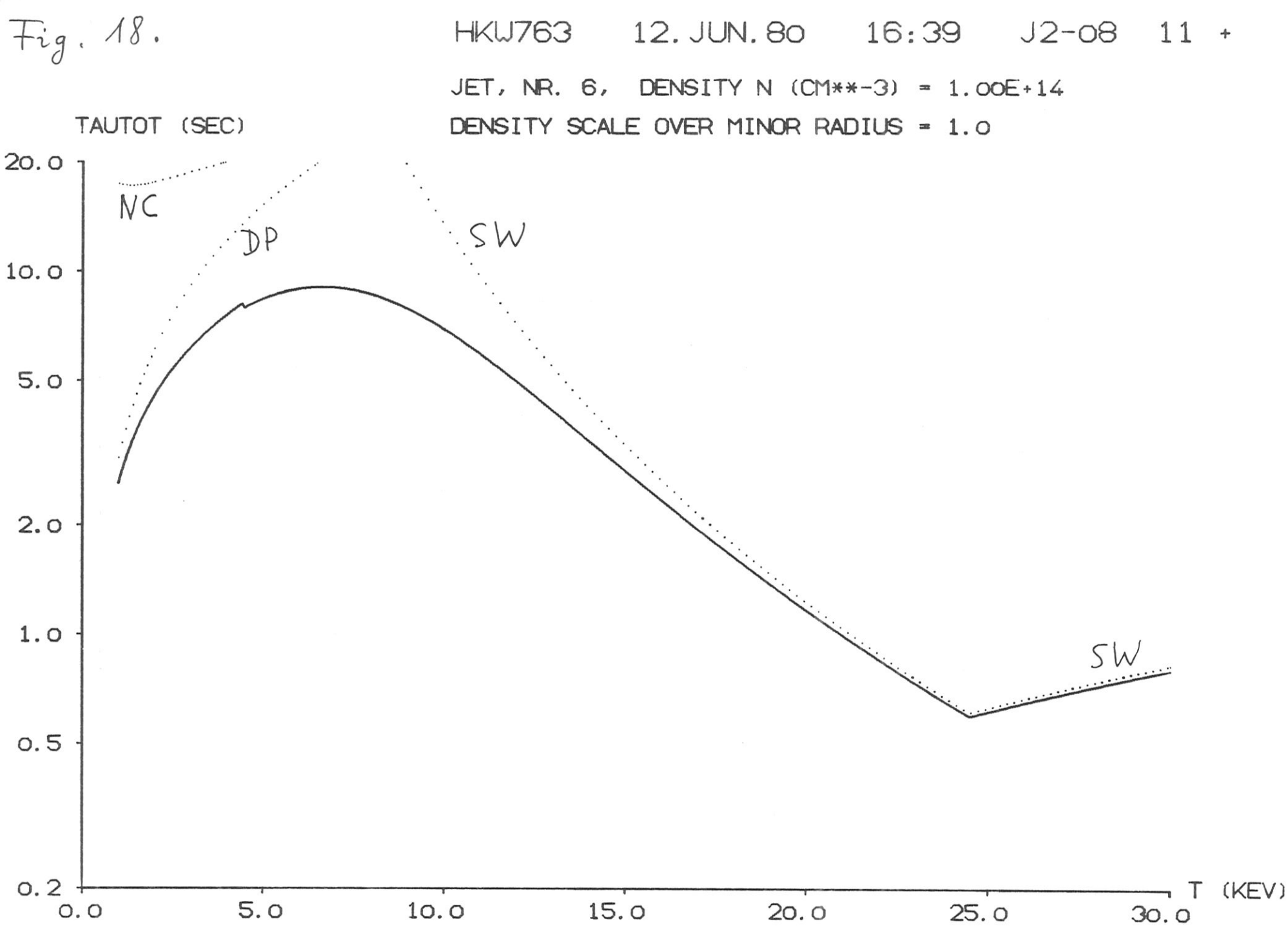
HKW763 12. JUN. 80 16:39 J2-08 11 +
JET, NR. 6, DENSITY N (CM**-3) = 1.00E+14
DENSITY SCALE OVER MINOR RADIUS = 1.0
TAUTOT (SEC)
20.0
10.0
5.0
2.0
1.0
0.5
0.2
NC
DP
SW
SW
0.0
5.0
10.0
15.0
20.0
25.0
30.0
T (KEV)

Fig. 19.

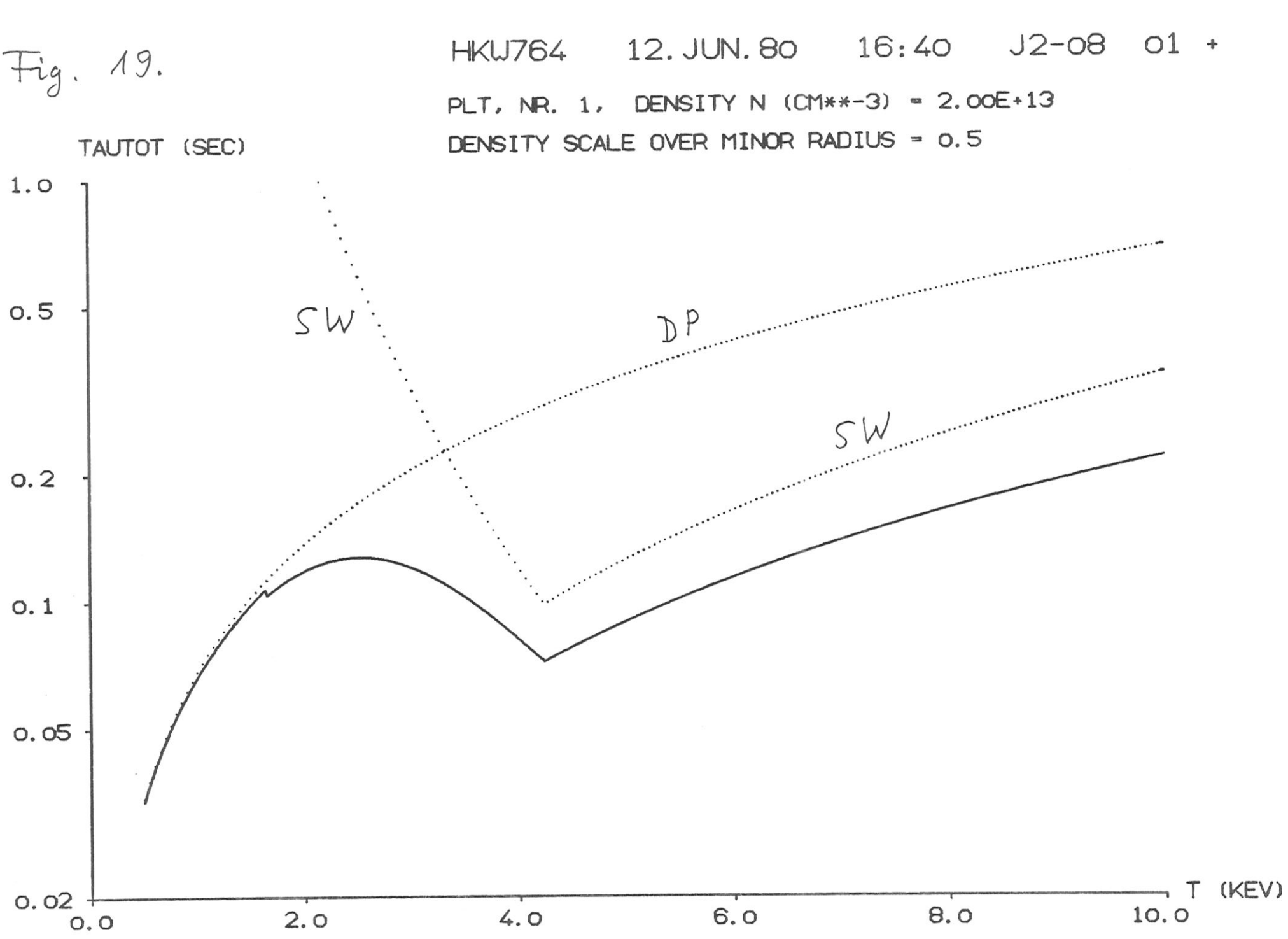
HKW764 12. JUN. 80 16:40 J2-08 01 +
PLT, NR. 1, DENSITY N (CM**-3) = 2.00E+13
DENSITY SCALE OVER MINOR RADIUS = 0.5
TAUTOT (SEC)
1.0
0.5
0.2
0.1
0.05
0.02
SW
DP
SW
0.0
2.0
4.0
6.0
8.0
10.0
T (KEV)

Fig. 20.

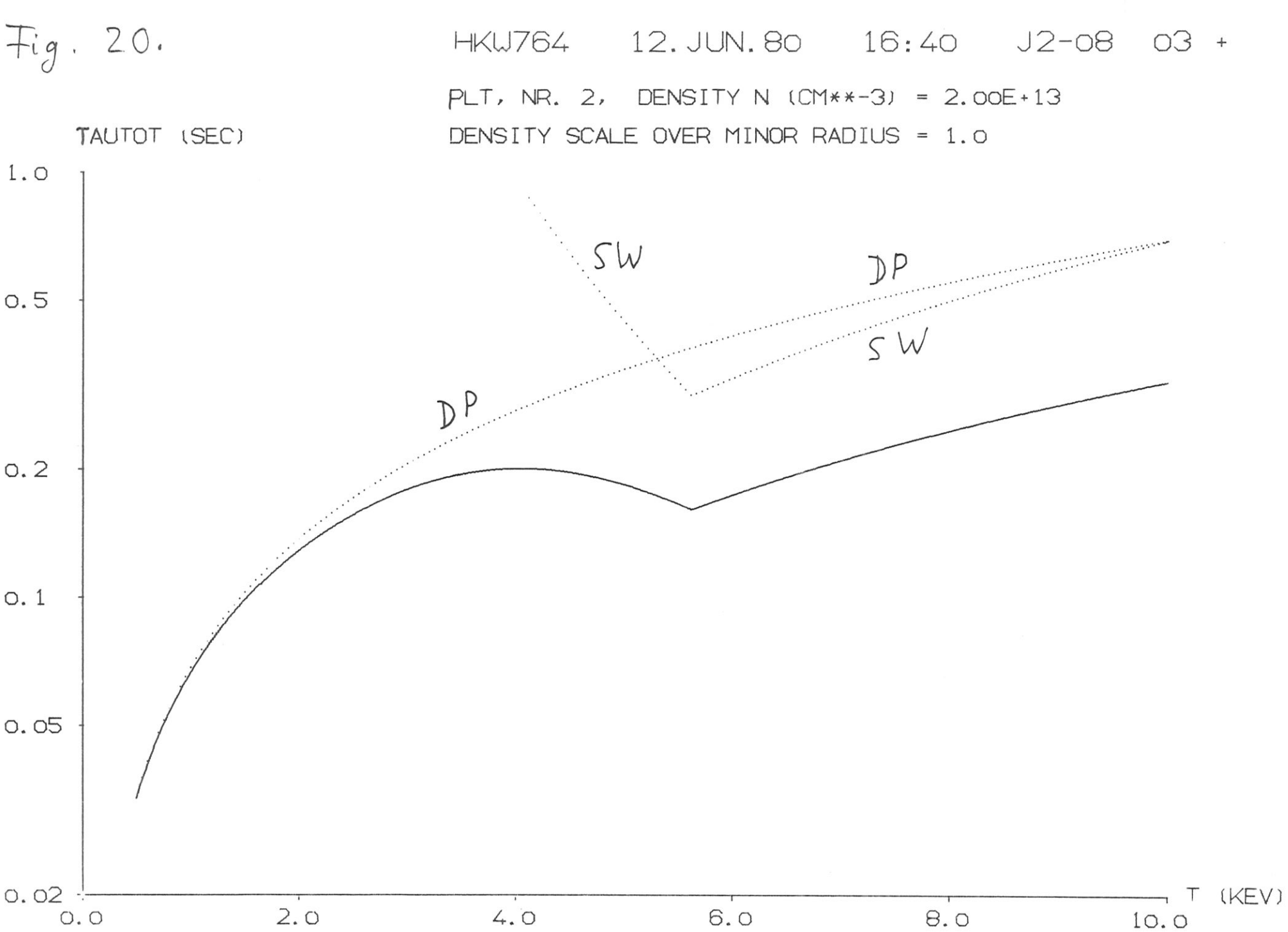
HKW764 12. JUN. 80 16:40 J2-08 03 +
PLT, NR. 2, DENSITY N (CM**-3) = 2.00E+13
DENSITY SCALE OVER MINOR RADIUS = 1.0
TAUTOT (SEC)
1.0
0.5
0.2
0.1
0.05
0.02
SW
DP
DP
SW
0.0
2.0
4.0
6.0
8.0
10.0
T (KEV)

Fig. 21.

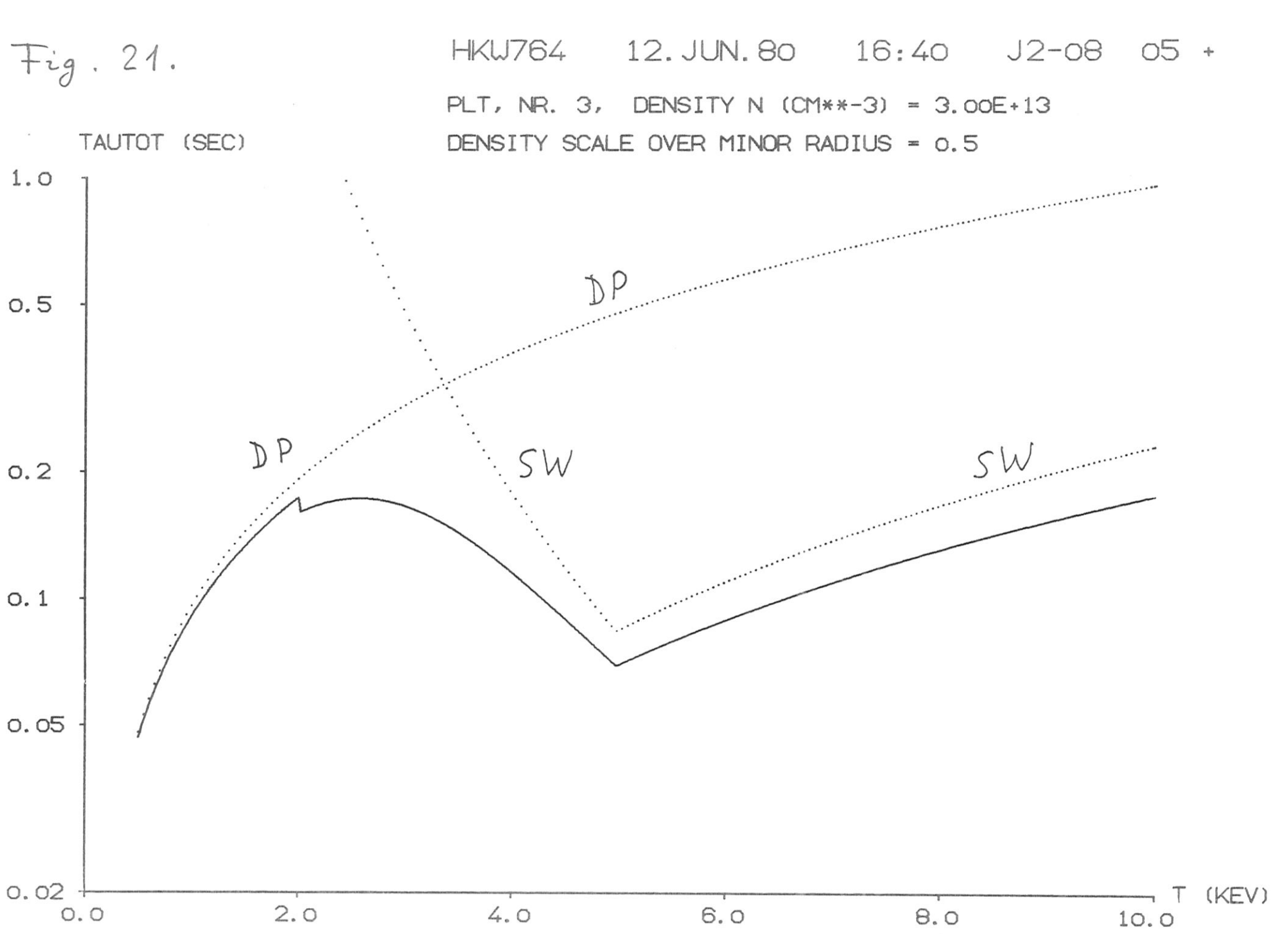
HKW764 12. JUN. 80 16:40 J2-08 05 +
PLT, NR. 3, DENSITY N (CM**-3) = 3.00E+13
DENSITY SCALE OVER MINOR RADIUS = 0.5
TAUTOT (SEC)
1.0
0.5
0.2
0.1
0.05
0.02
DP
DP
SW
SW
0.0
2.0
4.0
6.0
8.0
10.0
T (KEV)

Fig. 22.

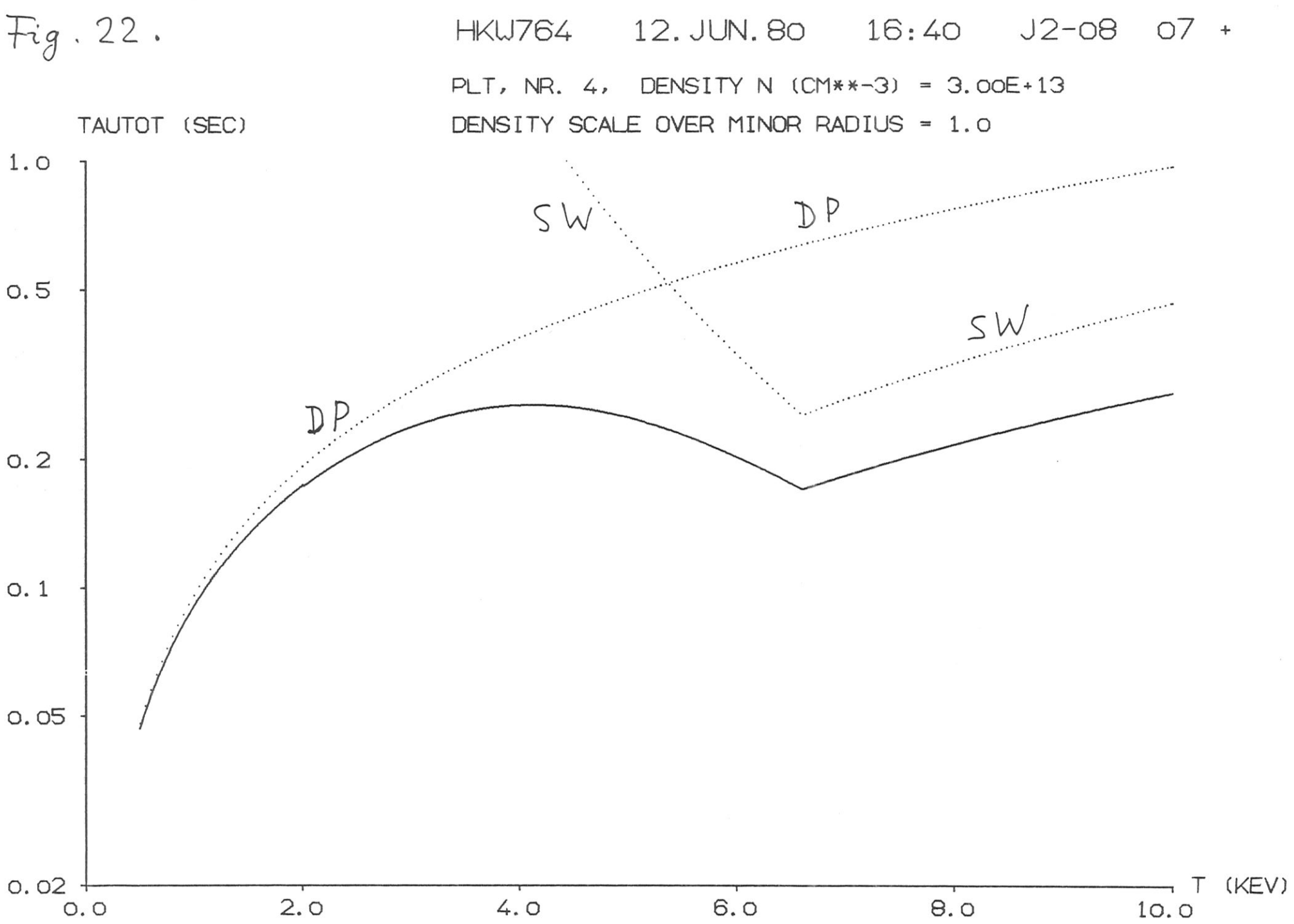
HKW764 12. JUN. 80 16:40 J2-08 07 +
PLT, NR. 4, DENSITY N (CM**-3) = 3.00E+13
DENSITY SCALE OVER MINOR RADIUS = 1.0
TAUTOT (SEC)
1.0
0.5
0.2
0.1
0.05
0.02
SW
DP
DP
SW
0.0
2.0
4.0
6.0
8.0
10.0
T (KEV)

Fig. 23.

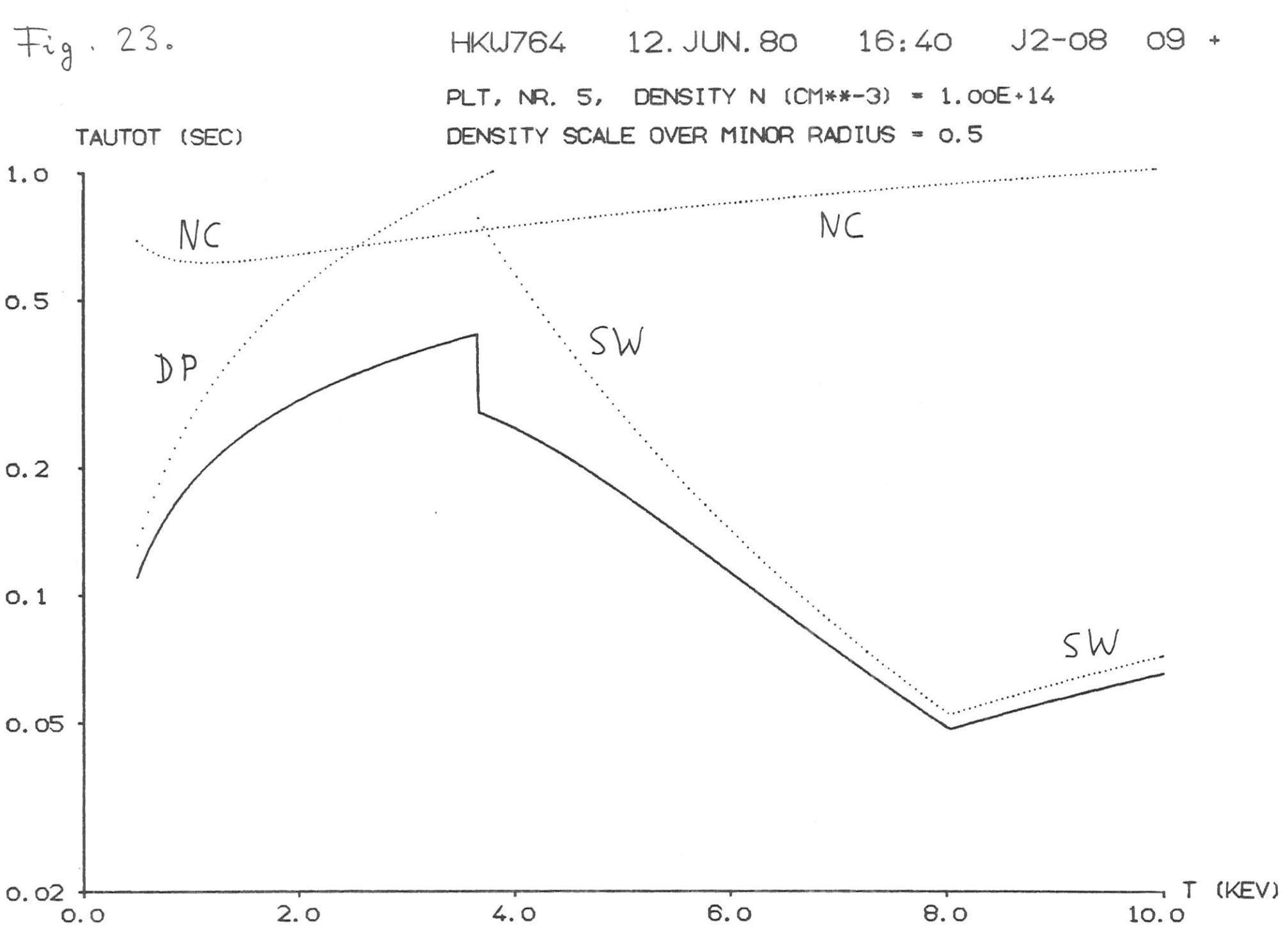
HKW764 12. JUN. 80 16:40 J2-08 09 +
PLT, NR. 5, DENSITY N (CM**-3) = 1.00E+14
DENSITY SCALE OVER MINOR RADIUS = 0.5
TAUTOT (SEC)
1.0
0.5
0.2
0.1
0.05
0.02
NC
NC
DP
SW
SW
0.0
2.0
4.0
6.0
8.0
10.0
T (KEV)

Fig. 24.

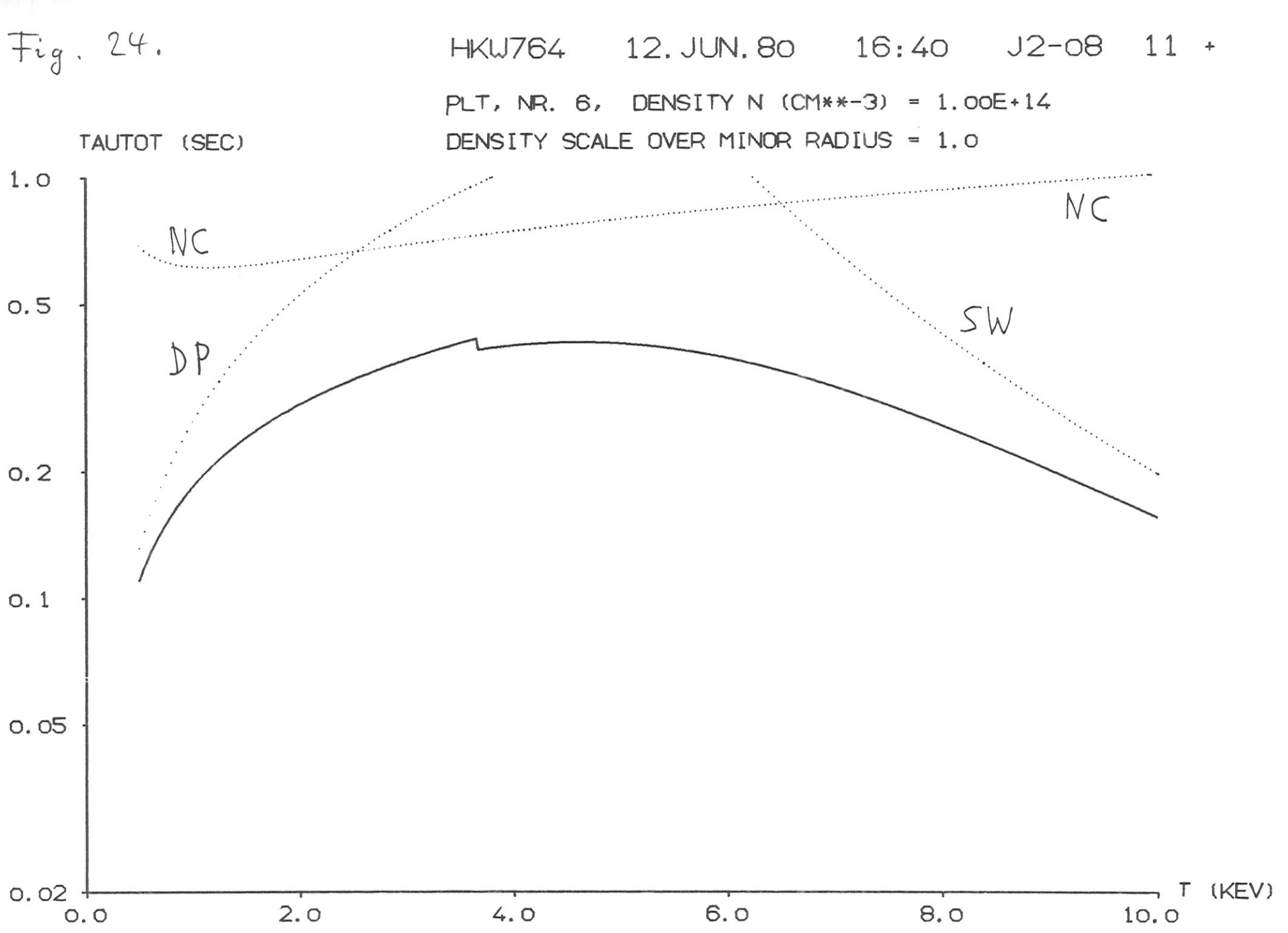
HKW764 12. JUN. 80 16:40 J2-08 11 +
PLT, NR. 6, DENSITY N (CM**-3) = 1.00E+14
DENSITY SCALE OVER MINOR RADIUS = 1.0
TAUTOT (SEC)
1.0
0.5
0.2
0.1
0.05
0.02
NC
NC
SW
DP
0.0
2.0
4.0
6.0
8.0
10.0
T (KEV)

Fig. 25.

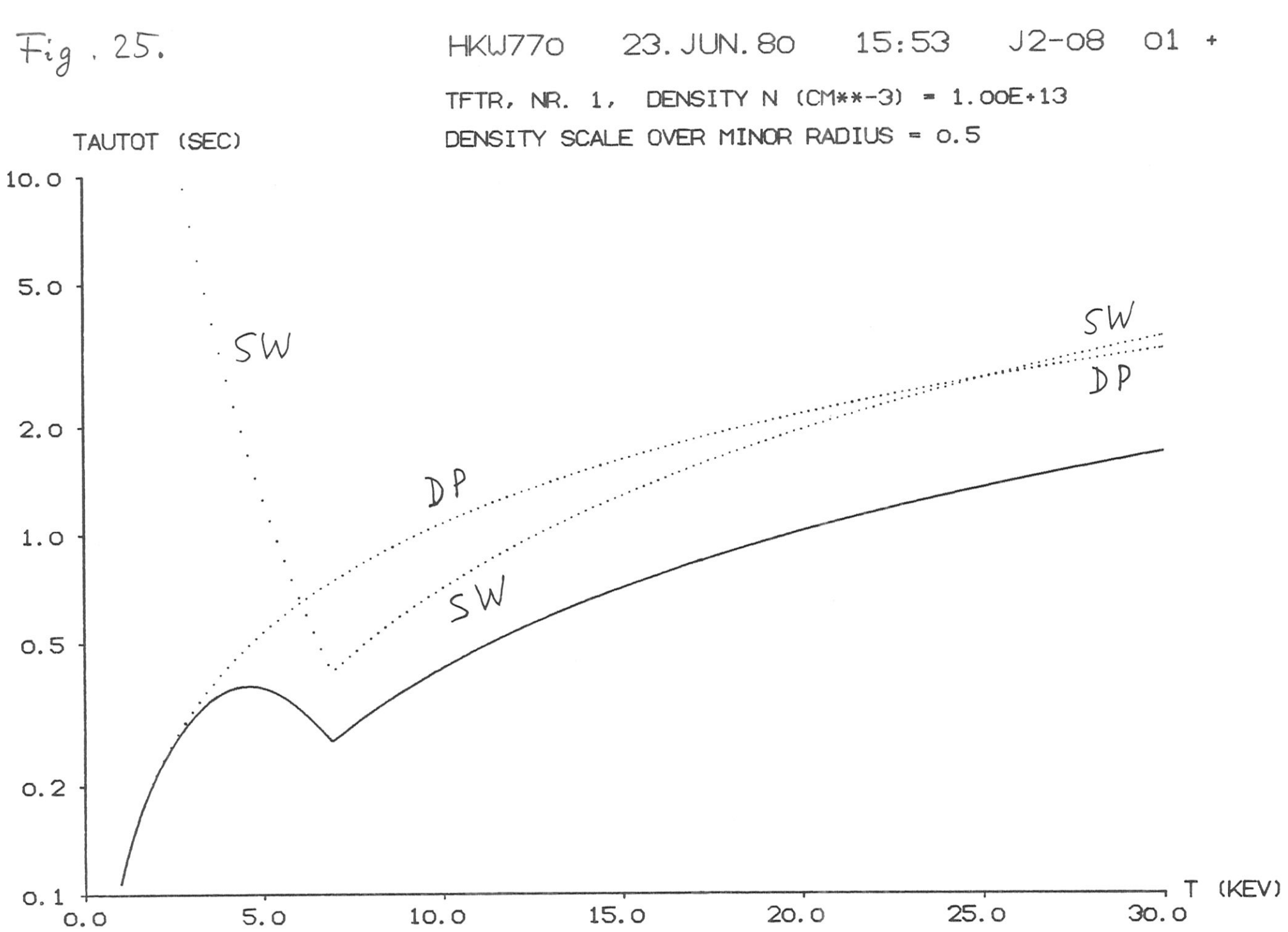
HKW770 23. JUN. 80 15:53 J2-08 01 +
TFTR, NR. 1, DENSITY N (CM**-3) = 1.00E+13
DENSITY SCALE OVER MINOR RADIUS = 0.5
TAUTOT (SEC)
10.0
5.0
2.0
1.0
0.5
0.2
0.1
SW
DP
SW
DP
SW
0.0
5.0
10.0
15.0
20.0
25.0
30.0
T (KEV)

Fig. 26.

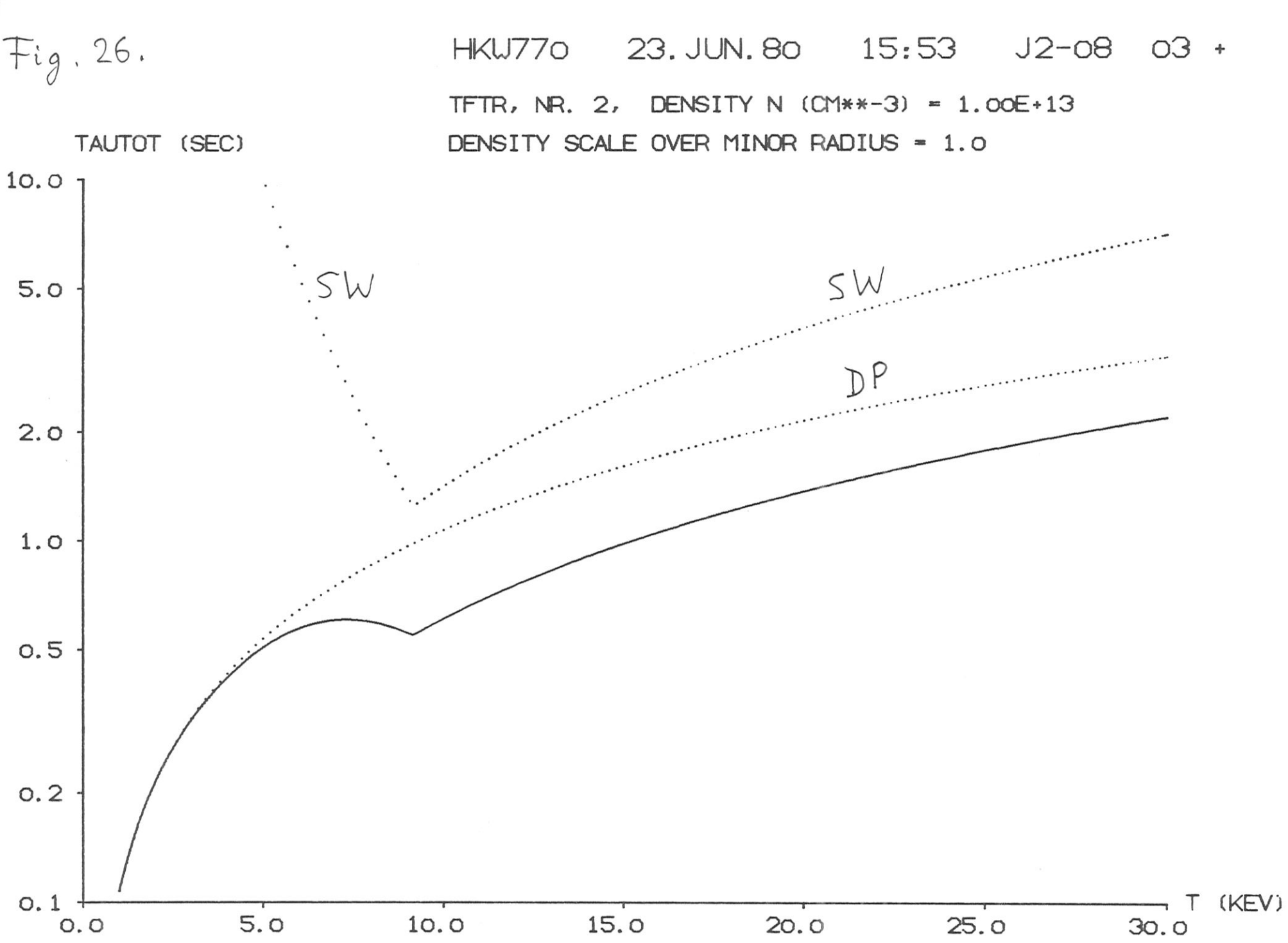
HKW77o 23. JUN. 8o 15:53 J2-08 03 +
TFTR, NR. 2, DENSITY N (CM**-3) = 1.ooE+13
DENSITY SCALE OVER MINOR RADIUS = 1.o
TAUTOT (SEC)
10.o
5.o
2.o
1.o
o.5
o.2
o.1
SW
SW
DP
0.0
5.o
10.o
15.o
20.o
25.o
3o.o
T (KEV)

Fig. 27.

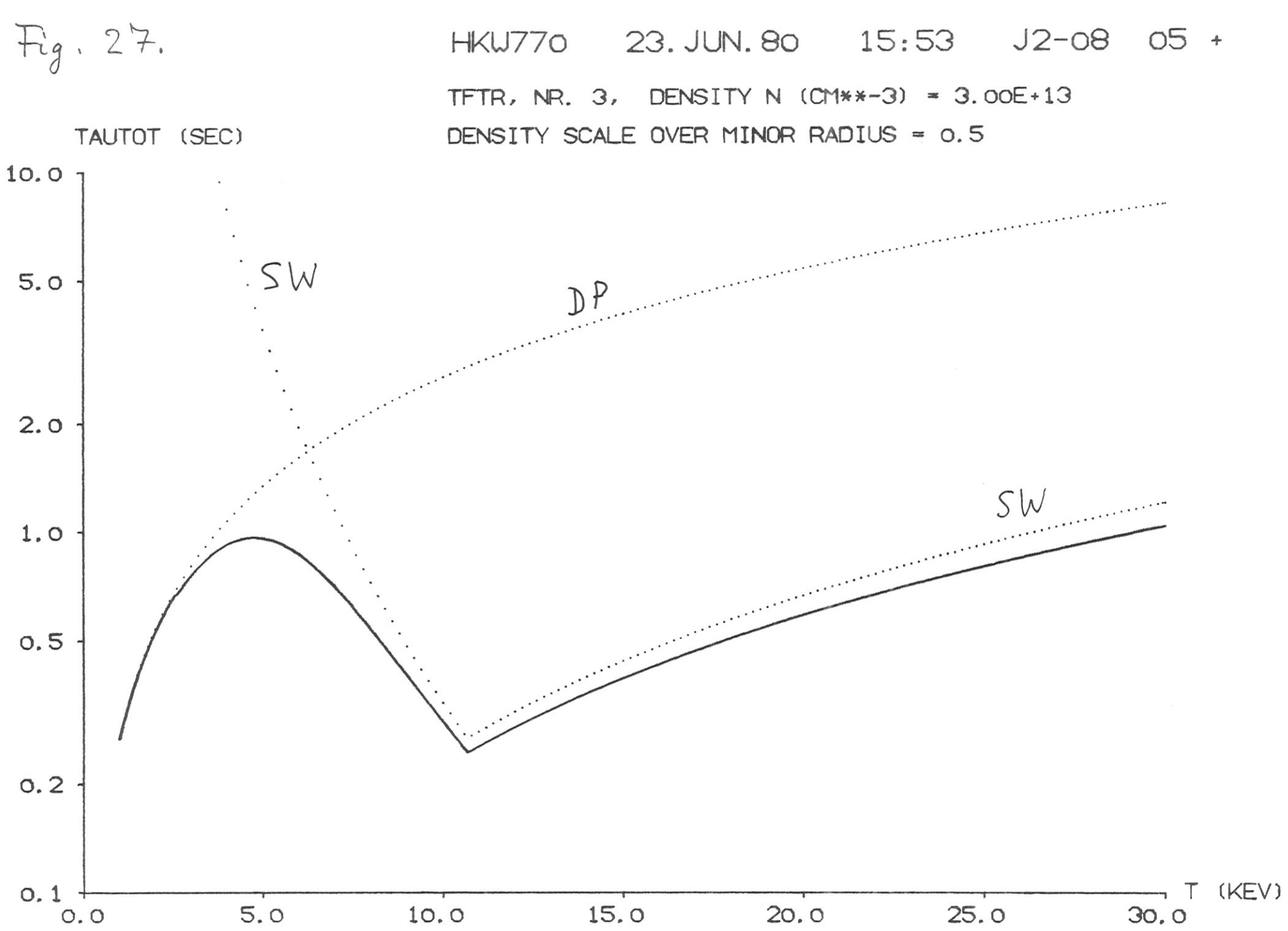
HKW770 23. JUN. 80 15:53 J2-08 05 +
TFTR, NR. 3, DENSITY N (CM**-3) = 3.00E+13
DENSITY SCALE OVER MINOR RADIUS = 0.5
TAUTOT (SEC)
10.0
5.0
2.0
1.0
0.5
0.2
0.1
SW
DP
SW
0.0
5.0
10.0
15.0
20.0
25.0
30.0
T (KEV)

Fig. 28.

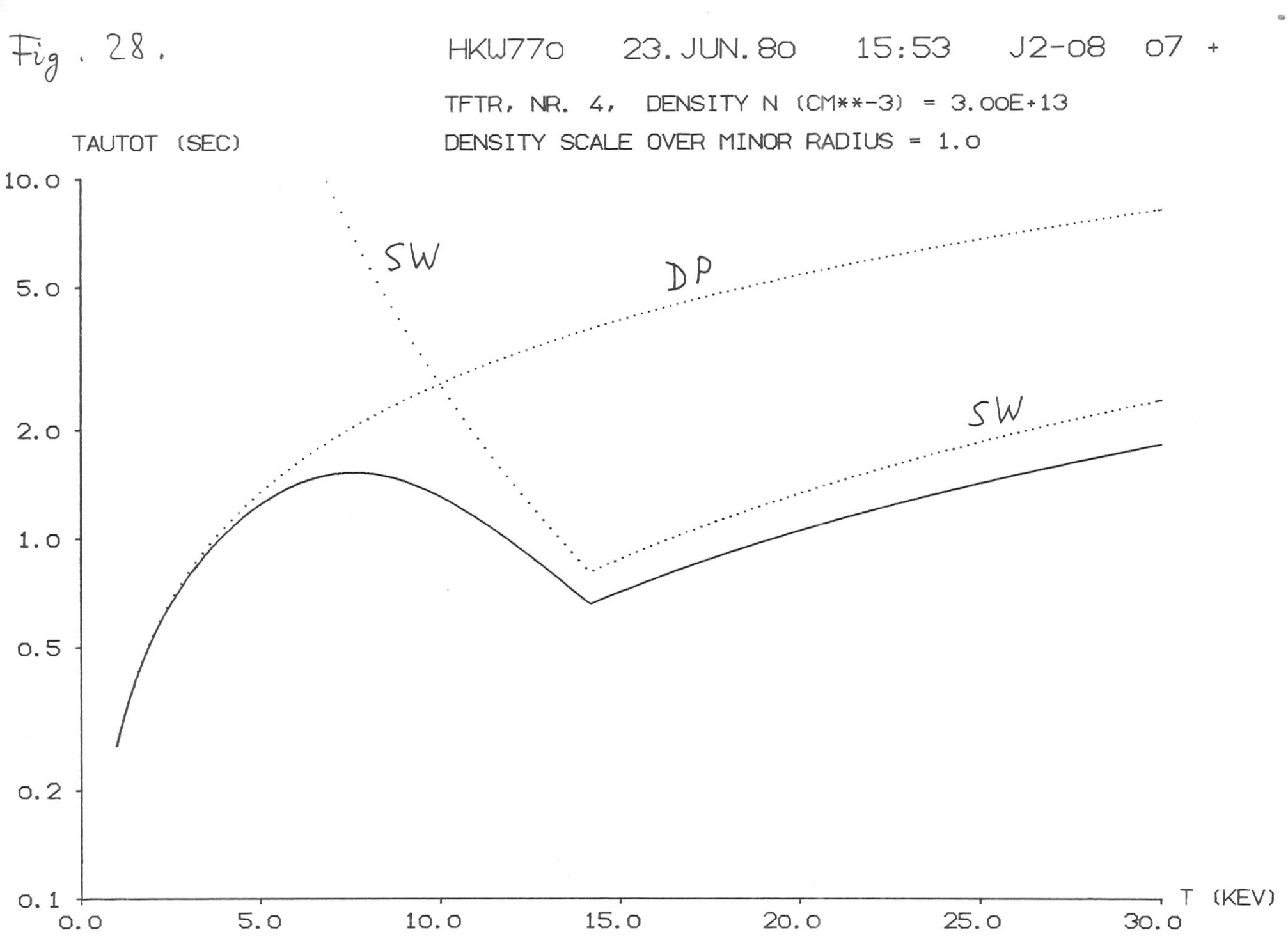
HKW770 23. JUN. 80 15:53 J2-08 07 +
TFTR, NR. 4, DENSITY N (CM**-3) = 3.00E+13
DENSITY SCALE OVER MINOR RADIUS = 1.0
TAUTOT (SEC)
10.0
5.0
2.0
1.0
0.5
0.2
0.1
SW
DP
SW
0.0
5.0
10.0
15.0
20.0
25.0
30.0
T (KEV)

Fig. 29.

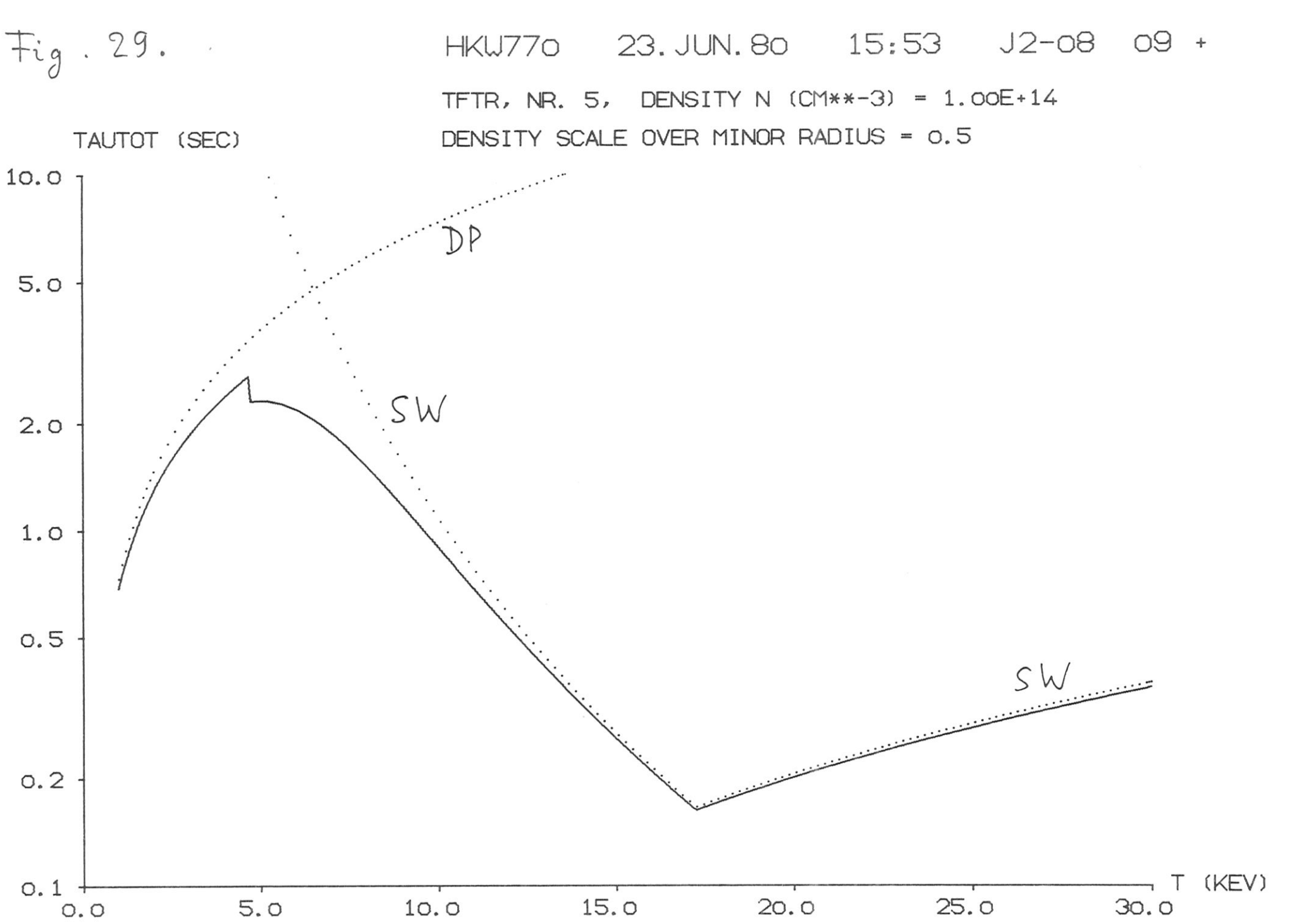
HKW770 23. JUN. 80 15:53 J2-08 09 +
TFTR, NR. 5, DENSITY N (CM**-3) = 1.00E+14
DENSITY SCALE OVER MINOR RADIUS = 0.5
TAUTOT (SEC)
10.0
5.0
2.0
1.0
0.5
0.2
0.1
DP
SW
SW
T (KEV)
0.0
5.0
10.0
15.0
20.0
25.0
30.0

Fig. 30.

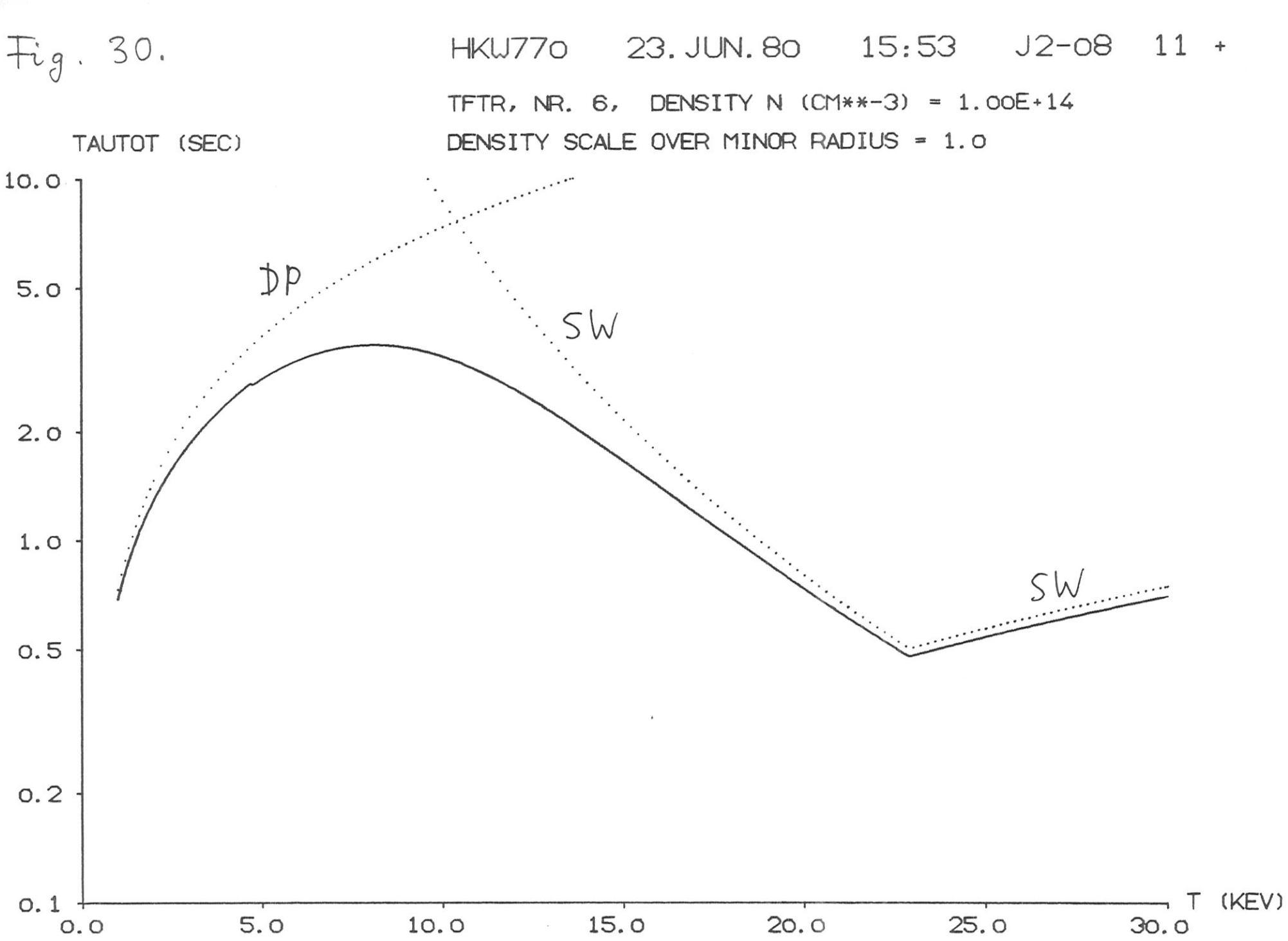
HKW77o 23. JUN. 80 15:53 J2-08 11 +
TFTR, NR. 6, DENSITY N (CM**-3) = 1.00E+14
DENSITY SCALE OVER MINOR RADIUS = 1.0
TAUTOT (SEC)
10.0
5.0
2.0
1.0
0.5
0.2
0.1
DP
SW
SW
0.0
5.0
10.0
15.0
20.0
25.0
30.0
T (KEV)

Fig. 31.

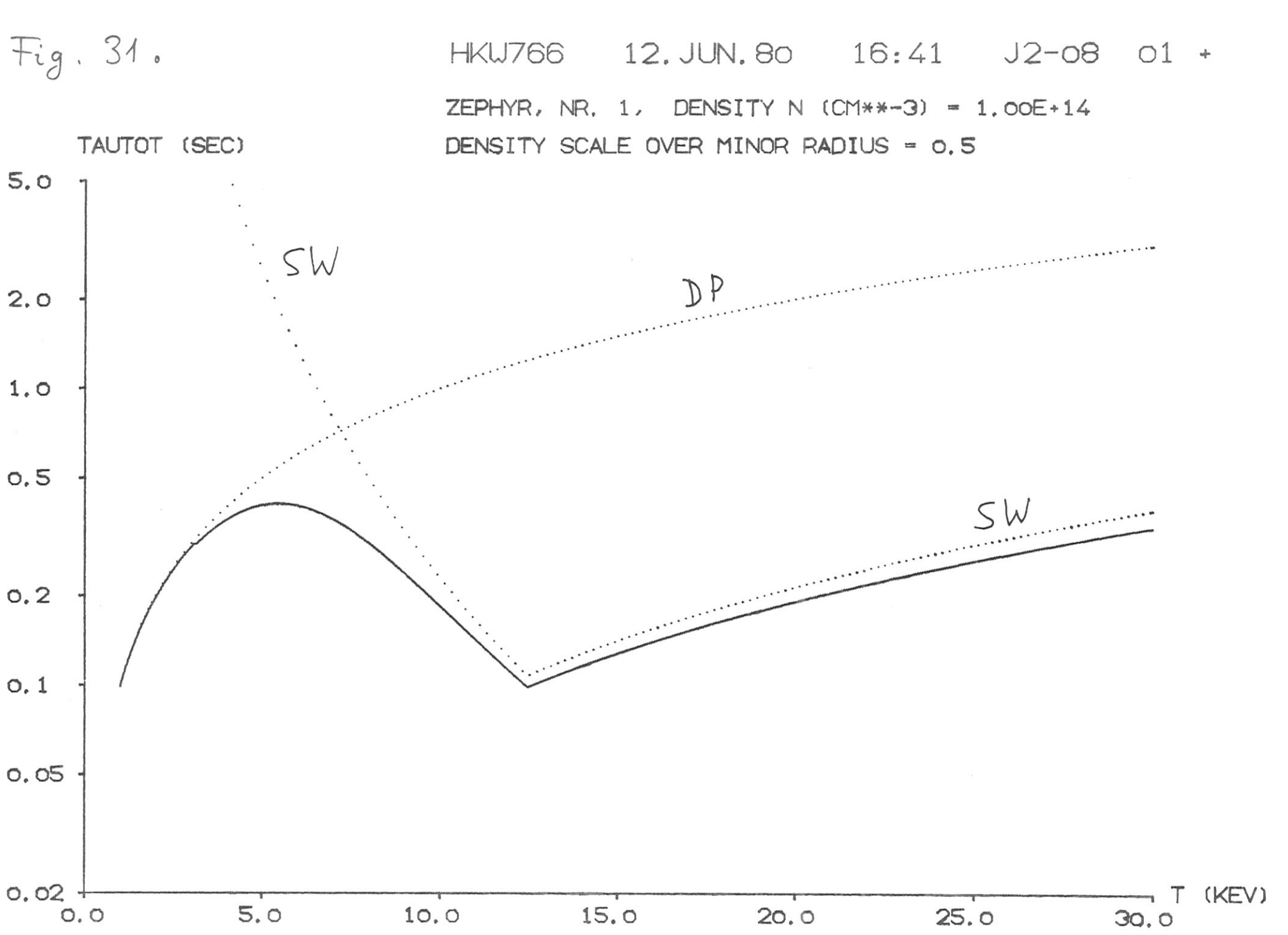
HKW766 12. JUN. 80 16:41 J2-08 01 +
ZEPHYR, NR. 1, DENSITY N (CM**-3) = 1.00E+14
DENSITY SCALE OVER MINOR RADIUS = 0.5
TAUTOT (SEC)
5.0
2.0
1.0
0.5
0.2
0.1
0.05
0.02
SW
DP
SW
0.0
5.0
10.0
15.0
20.0
25.0
30.0
T (KEV)

Fig. 32.

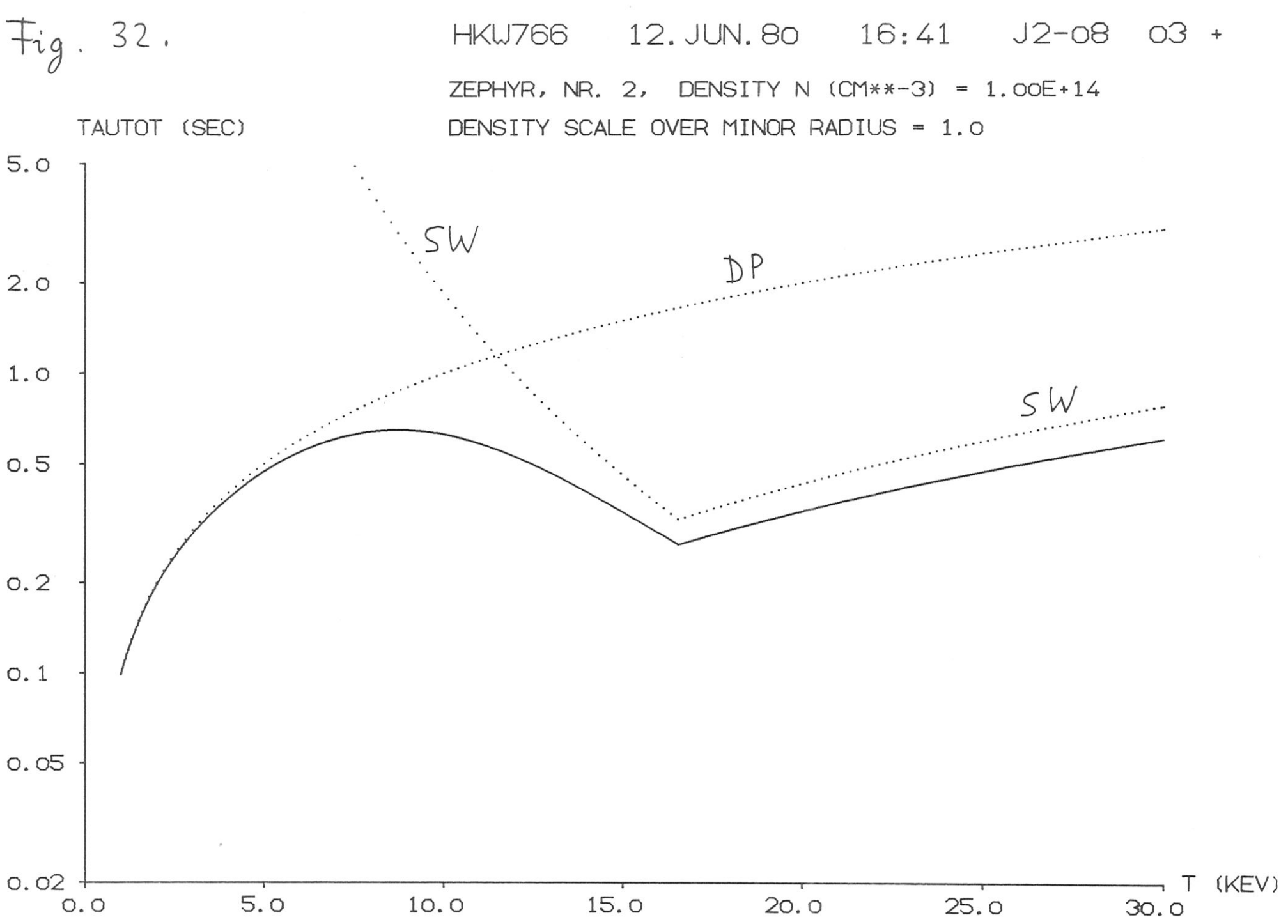
HKW766 12. JUN. 80 16:41 J2-08 03 +
ZEPHYR, NR. 2, DENSITY N (CM**-3) = 1.00E+14
DENSITY SCALE OVER MINOR RADIUS = 1.0
TAUTOT (SEC)
5.0
2.0
1.0
0.5
0.2
0.1
0.05
0.02
SW
DP
SW
0.0
5.0
10.0
15.0
20.0
25.0
30.0
T (KEV)

Fig. 33.

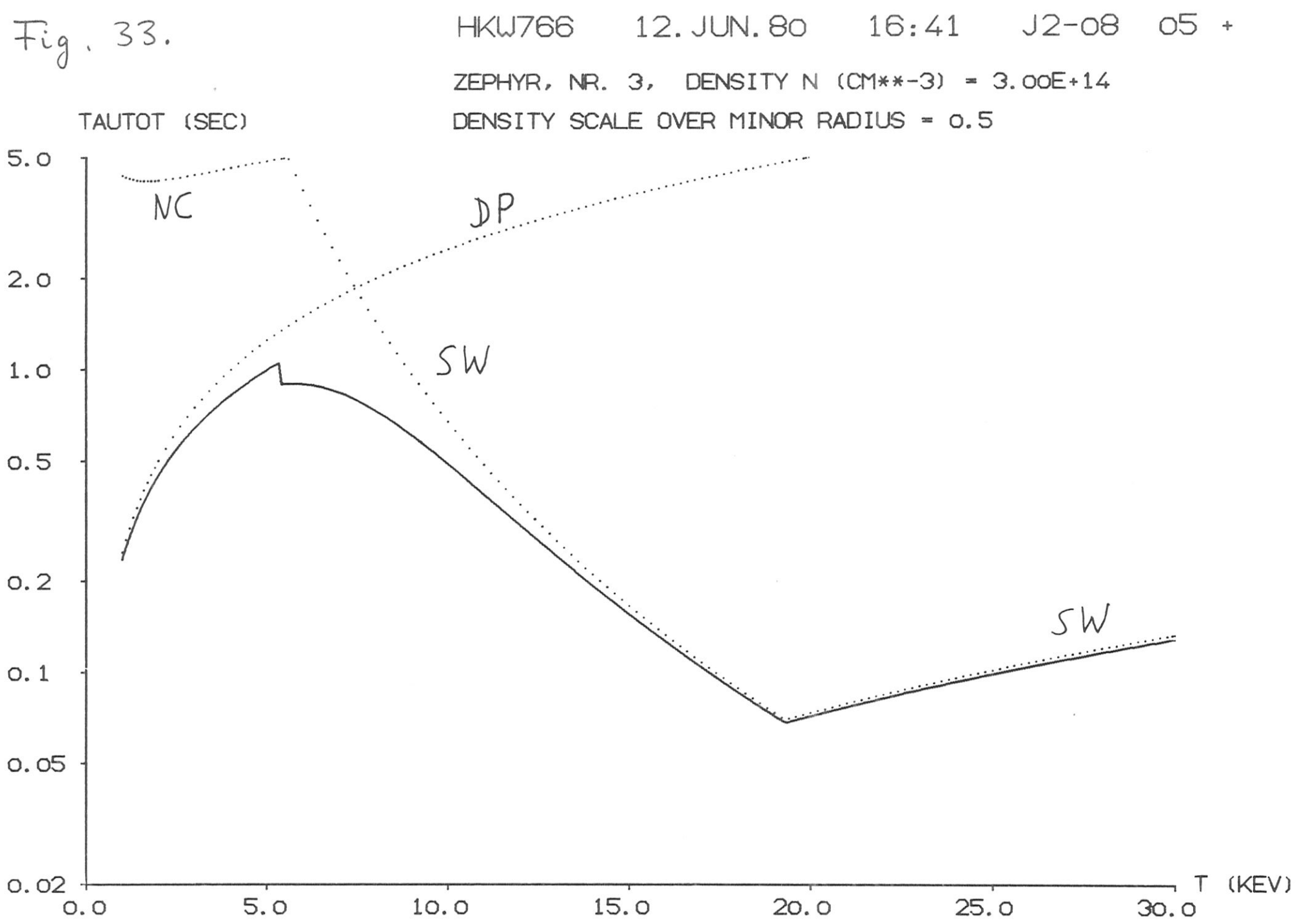
HKW766 12. JUN. 80 16:41 J2-08 05 +
ZEPHYR, NR. 3, DENSITY N (CM**-3) = 3.00E+14
DENSITY SCALE OVER MINOR RADIUS = 0.5
TAUTOT (SEC)
5.0
2.0
1.0
0.5
0.2
0.1
0.05
0.02
NC
DP
SW
SW
T (KEV)
0.0
5.0
10.0
15.0
20.0
25.0
30.0

Fig. 34.

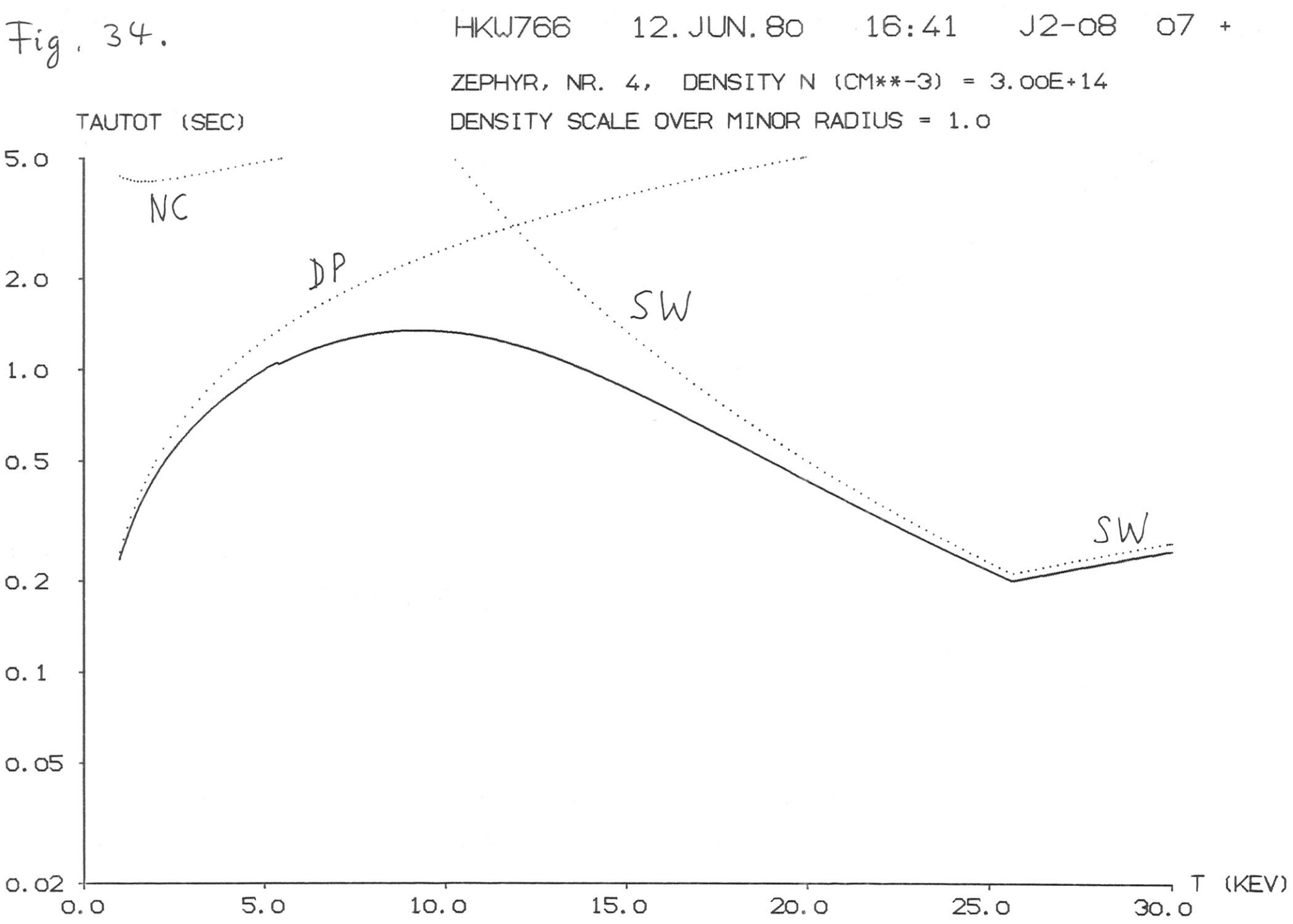
HKW766 12. JUN. 80 16:41 J2-08 07 +
ZEPHYR, NR. 4, DENSITY N (CM**-3) = 3.00E+14
DENSITY SCALE OVER MINOR RADIUS = 1.0
TAUTOT (SEC)
5.0
2.0
1.0
0.5
0.2
0.1
0.05
0.02
NC
DP
SW
SW
0.0
5.0
10.0
15.0
20.0
25.0
30.0
T (KEV)

Fig. 35.

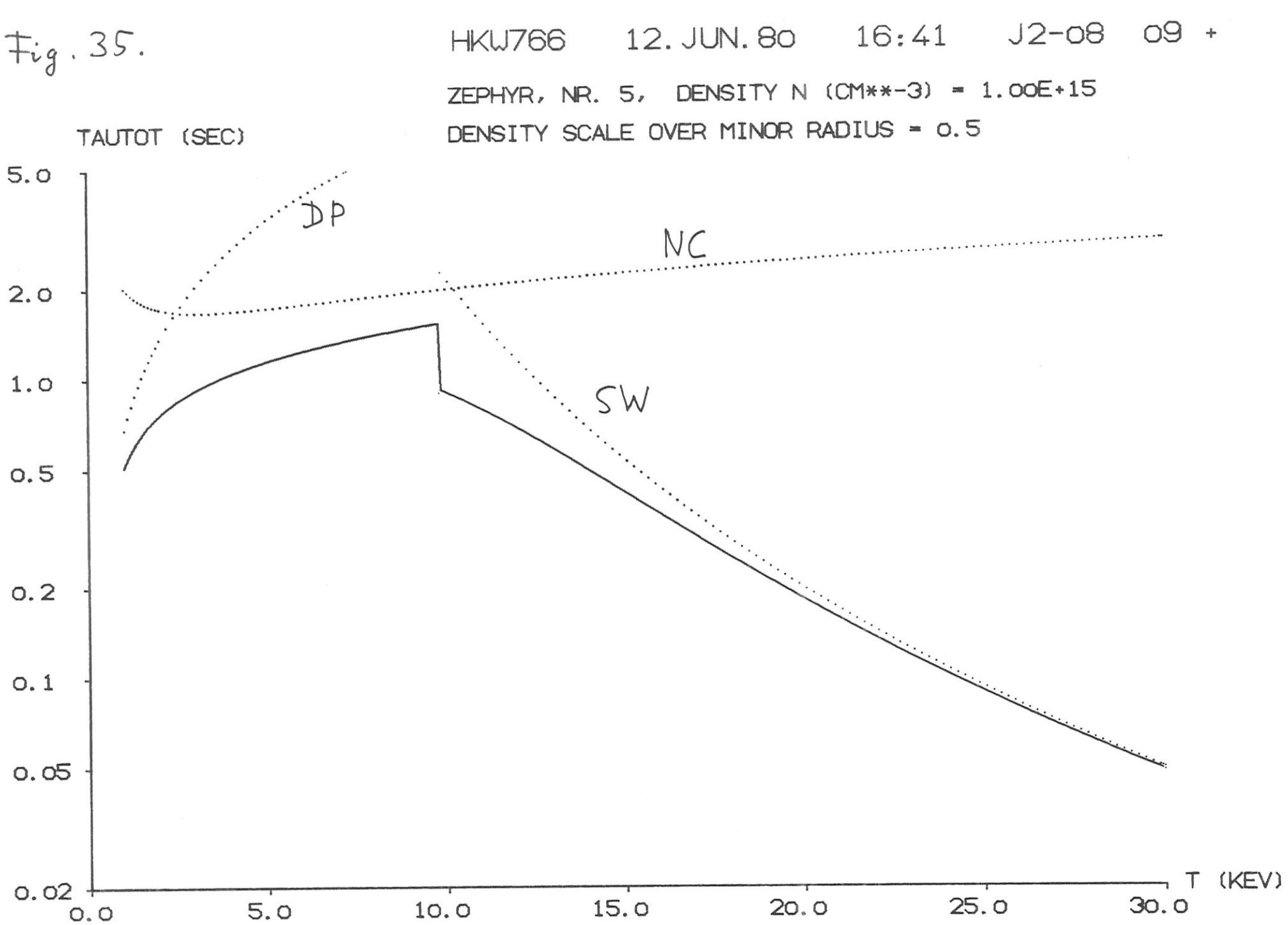
HKW766 12. JUN. 80 16:41 J2-08 09 +
ZEPHYR, NR. 5, DENSITY N (CM**-3) = 1.00E+15
DENSITY SCALE OVER MINOR RADIUS = 0.5
TAUTOT (SEC)
5.0
2.0
1.0
0.5
0.2
0.1
0.05
0.02
DP
NC
SW
0.0
5.0
10.0
15.0
20.0
25.0
30.0
T (KEV)

Fig. 36.

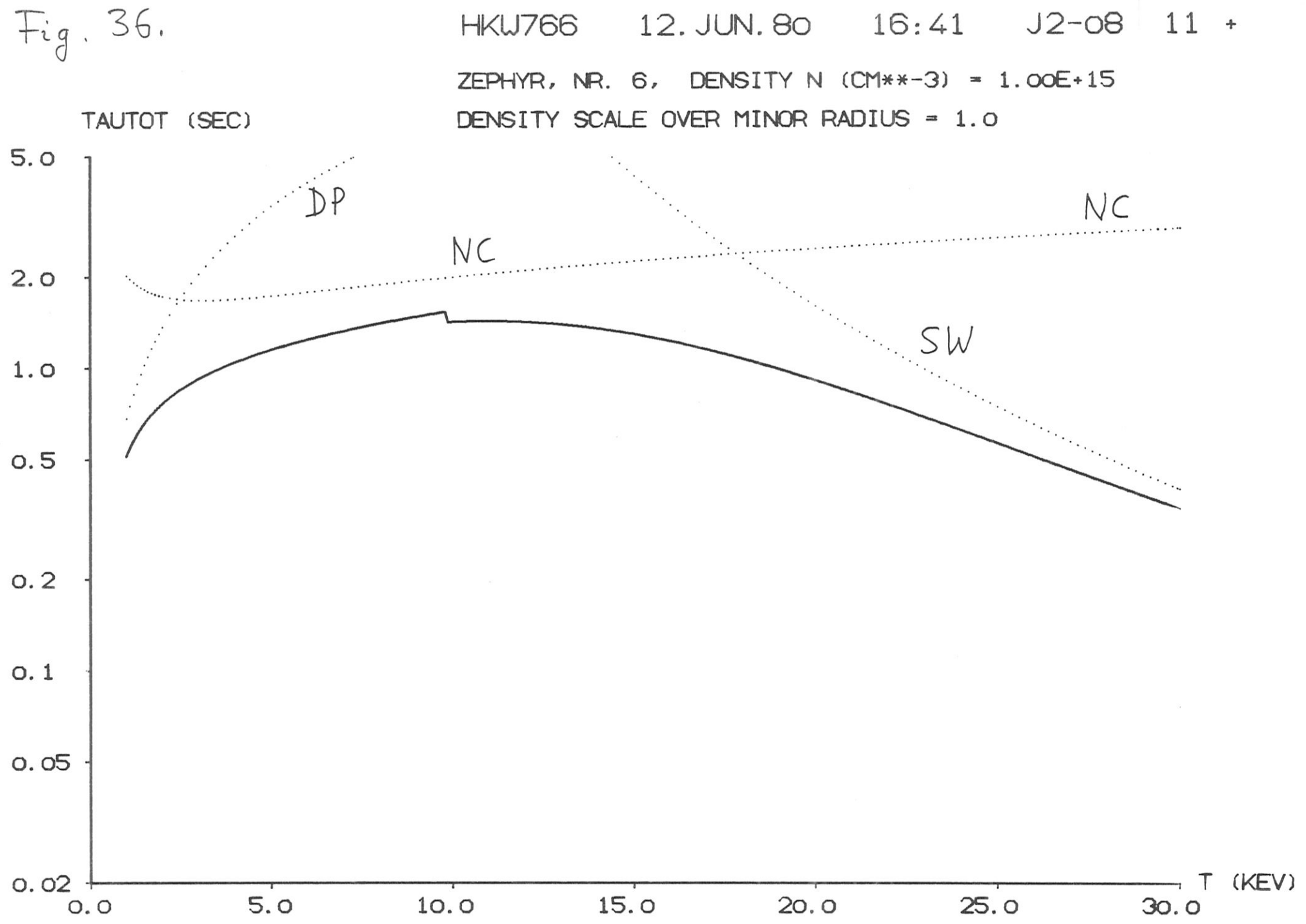
HKW766 12. JUN. 80 16:41 J2-08 11 +
ZEPHYR, NR. 6, DENSITY N (CM**-3) = 1.00E+15
DENSITY SCALE OVER MINOR RADIUS = 1.0
TAUTOT (SEC)
5.0
2.0
1.0
0.5
0.2
0.1
0.05
0.02
DP
NC
NC
SW
0.0
5.0
10.0
15.0
20.0
25.0
30.0
T (KEV)